

1
2
3
4
5 **DYNAMIC EFFECTIVE THICKNESS IN LAMINATED-GLASS BEAMS AND**
6
7 **PLATES**

8
9
10 M. López-Aenlle^{a*}, F. Pelayo^a

11
12 ^a**Department of Construction and Manufacturing Engineering, University of**
13 **Oviedo, Campus de Gijón, Zona Oeste, Edificio 7, 33203, Gijón, Spain.**

14
15
16
17 ^{*}**corresponding author; E-mail: aenlle@uniovi.es**

18 **Phone: +34985 182057, Fax: +34985 18 2433**

19
20
21
22
23
24 **Abstract**

25
26
27 In recent years, several equations have been proposed to calculate deflections and
28 stresses in laminated-glass beams and plates under static loading using the concept of
29 effective thickness, which consists of calculating the thickness of a monolithic element
30 with equivalent bending properties to a laminated element. Recently, an effective
31 thickness for the dynamic behaviour of laminated-glass beams has been proposed to
32 enable the modal parameters (natural frequencies, loss factors and mode shapes) to be
33 determined using an equivalent monolithic model. In the present paper, the technique
34 has been extended to the two-dimensional case of rectangular laminated-glass plates and
35 the steps needed to estimate the modal parameters of laminated-glass elements using
36 this methodology are presented. The dynamic effective thickness concept has been
37 validated by experimental tests made on a laminated-glass beam and a laminated-glass
38 plate. The results show that good accuracy is achieved in the natural frequencies and
39 mode shapes but high scatter is encountered in the loss factors.

40
41
42
43
44
45
46
47
48
49
50
51 **Keywords:** A. Laminated glass ; B. Operational Modal Analysis ; C. Effective
52 Thickness; D. Viscoelasticity.
53
54
55
56
57
58
59
60
61
62
63
64
65

1
2
3
4 NOMENCLATURE
5
6

7 D Flexural Stiffness in plates
8

9
10 E Young modulus
11

12 E_{eff} Effective Young modulus
13
14

15 E_1 Young's modulus of glass layer 1
16
17

18 E_3 Young's modulus of glass layer 3
19
20

21 EI^* Complex flexural stiffness in beams
22
23

24 $E_2^*(\omega)$ Complex tensile modulus for the polymeric interlayer
25
26

27 $E'(\omega)$ Real component of the tensile complex modulus (storage)
28
29

30 $E''(\omega)$ Imaginary component of the tensile complex modulus (loss)
31
32

33 EIT $E_1I_1 + E_3I_3$
34
35

36 $E_2(t)$ Viscoelastic relaxation tensile modulus for polymeric interlayer
37
38

39 E_∞^2 Equilibrium tensile modulus for the polymeric interlayer
40
41

42 $G_2(t)$ Viscoelastic relaxation shear modulus for the polymeric interlayer
43
44

45 $G_2^*(\omega)$ Complex shear modulus for the polymeric interlayer
46
47

48 G_0 Glassy shear modulus
49
50

51 H_1 Thickness of glass layer 1 in laminated glass
52
53

54 H_2 Thickness of polymeric layer in laminated glass
55
56

57 H_3 Thickness of glass layer 3 in laminated glass
58
59

1
2
3
4
5
6
7
8
9
10
11
12
13
14
15
16
17
18
19
20
21
22
23
24
25
26
27
28
29
30
31
32
33
34
35
36
37
38
39
40
41
42
43
44
45
46
47
48
49
50
51
52
53
54
55
56
57
58
59
60
61
62
63
64
65

$$H_0 = H_2 + \left(\frac{H_1+H_3}{2}\right)$$

I Second moment of area

$$I_1 = \frac{H_1^3}{12}$$

$$I_3 = \frac{H_3^3}{12}$$

$$I_T = I_1 + I_3 = \frac{H_1^3+H_3^3}{12}$$

$K(t)$ Viscoelastic bulk modulus

L Length of a glass beam

T Temperature

T_0 Reference temperature

$$Y = \frac{H_0^2 E_1 H_1 E_3 H_3}{E I_T (E_1 H_1 + E_3 H_3)}$$

$$Y_1 = \frac{12 H_0^2 H_1 H_3}{(H_1^3 + H_3^3)(H_1 + H_3)}$$

LOWERCASE LETTERS

a_T Shift factor

b Width of a glass beam

e_i Modulus coefficient in Prony's series viscoelastic model

$g(x)$ Shape function (Galuppi and Royer Carfagni model)

g_M^* Shear parameter M&Ms Model

1
2
3
4
5
6
7
8
9
10
11
12
13
14
15
16
17
18
19
20
21
22
23
24
25
26
27
28
29
30
31
32
33
34
35
36
37
38
39
40
41
42
43
44
45
46
47
48
49
50
51
52
53
54
55
56
57
58
59
60
61
62
63
64
65

g_R^* Shear parameter RKU model

i Imaginary unit

k_I Wavenumber

k_M^* Complex wave number

\bar{m} Mass per unit area

t Time

w Deflection

GREEK LETTERS

Ω^* Non-dimensional complex frequency

β Bucking ratio for a beam

ζ Modal damping ratio

η Loss factor

η_2 Loss factor of the polymeric interlayer of laminated glass

ν_i Poisson ratio of the i-th glass layer

ρ_i Mass density of the i-th glass layer

τ_i Time coefficient in Prony's series viscoelastic model

ω Frequency

1
2
3
4 1 INTRODUCTION
5
6

7 Laminated glass is a sandwich or layered material consisting of two or more plies of
8 monolithic glass with one or more interlayers of a polymeric material. Thus, a
9 laminated-glass element (beam, plate, etc.) is a composite material which combines the
10 properties of the glass with the benefits of a highly elastic polymeric material, i.e. the
11 structural behaviour of laminated glass is that of a composite structure. The glass layers
12 may be either normal annealed, heat-strengthened, chemically strengthened or tempered
13 glass. When the cross-section is made of different glasses (e.g. one layer of annealed
14 glass and the other of tempered glass) it is called a hybrid laminated-glass element.
15 However, the treatments affect the ultimate strength but not the Young modulus, and
16 therefore no distinction is made concerning the type of glass if the calculations are made
17 prior to glass breakage. All polymeric interlayers are viscoelastic in nature [1], i.e. their
18 mechanical properties are frequency (or time) and temperature dependent. Polyvinyl
19 butyral (PVB) is the most commonly used interlayer material and is marketed in
20 thicknesses of 0.38 mm or a multiple of this value (0.76 mm, 1.12 mm, 1.52 mm).
21 However, the new ionoplastic interlayers improve the mechanical properties of
22 laminated glass and maintains a significant advantage (higher stiffness and strength)
23 over the PVB for a large range of temperatures [1] . This interlayer material is now in
24 flat sheet form, in thicknesses of 0.89, 1.52, 2.27, and 3.05 mm, and as rolled sheeting,
25 at 0.89 mm thickness. The simplest laminated-glass configuration consists of three
26 layers: two monolithic glass plies and a polymeric core (see Fig. 1).
27
28
29
30
31
32
33
34
35
36
37
38
39
40
41

42 The response of laminated-glass elements varies between two borderlines [2]: 1) The
43 layered limit corresponding to the case when the beam consists of free-sliding glass
44 plies and 2) the monolithic limit, when the Euler–Bernoulli assumptions hold (plane
45 sections remain plane) for the entire section of the laminated-glass element (the
46 response of the composite beam approaches that of a homogeneous glass beam with an
47 equal cross-section) [3-4]. As the tensile modulus of the PVB is far less in comparison
48 with that corresponding to glass, significant transverse shear appears in the viscoelastic
49 layer [1, 8, 10].
50
51
52
53
54
55
56
57
58
59
60
61
62
63
64
65

1
2
3
4 In the analytical and numerical models, glass mechanical behaviour is usually modeled
5 as linear-elastic prior to glass breakage, whereas the polymeric interlayer is
6 characterized as linear-viscoelastic. Laminated glass is easy to assemble in a finite-
7 element model but many small 3D elements are needed to mesh accurately, which, on
8 the other hand, are very high time consuming. In the last few years, some papers have
9 been published on the calculation of laminated-glass elements, examining the concept of
10 effective thickness [1, 3, 4, 8]. The method consists of calculating the thickness of a
11 monolithic element with bending properties equivalent to those of the laminated one.
12 The effective thickness can then be used in analytical equations and simplified finite-
13 element models instead of the laminated-glass element [9].
14
15
16
17
18
19
20
21

22 The aim of the present paper is to propose a simplified method to estimate the modal
23 parameters of rectangular laminated-glass plates while avoiding the use of finite-
24 element models or complicated analytical models. The method is based on the dynamic
25 effective thickness proposed in a previous paper [9] for laminated-glass beams, which is
26 here extended to the two-dimensional case of rectangular laminated-glass plates. An
27 alternative to the effective thickness is the concept of effective Young modulus, which
28 can be used interchangeably for laminated-glass elements with the same accuracy. This
29 technique can be applied to three-layered laminated-glass plates with glass showing a
30 linear elastic behaviour and the polymeric core showing viscoelastic behaviour. Thus
31 the glass layers can be made of different types of glass (annealed, tempered, heat-
32 strengthened, etc.), and the traditional cores (PVB, ionoplastic, etc.) can be considered
33 in this model. In this paper, the modal parameters (natural frequencies, loss factors, and
34 mode shapes) of a 1400 x 1000 x 16 mm laminated-glass plate pin-supported at the four
35 corners, and of a beam 1 m long and 12 mm thick, both the beam and the plate with
36 annealed glass plies and PVB core, were estimated using the effective thickness
37 concept. For the validation of the model, operational modal tests were performed on the
38 beam and the plate, and the modal parameters identified from the experimental
39 responses were compared with those predicted using the effective thickness concept.
40
41
42
43
44
45
46
47
48
49
50
51
52
53
54
55
56
57
58
59
60
61
62
63
64
65

1
2
3
4 2 STATE OF THE ART
5
6

7 2.1 Viscoelastic Behaviour
8

9
10 The mechanical properties of a linear-viscoelastic material are frequency (or time) and
11 temperature dependent [11]. In the frequency domain, the complex tensile modulus,
12 $E_2^*(\omega)$, at temperature T is given by:
13
14

15
16
17
$$E_2^*(\omega, T) = E_2'(\omega, T) + i \cdot E_2''(\omega, T) = E_2'(\omega, T)(1 + i \cdot \eta_2(\omega, T)) \quad (1)$$

18
19

20
21 where superscript ‘*’ indicates complex, ω represents the frequency, i is the imaginary
22 unit, $E_2'(\omega, T)$ and $E_2''(\omega, T)$ are the storage and the loss tensile moduli, respectively,
23 and
24
25

26
27
28
29
$$\eta_2(\omega) = \frac{E_2''(\omega, T)}{E_2'(\omega, T)} \quad (2)$$

30
31
32

33
34 is the loss factor that relates the two moduli. The subscript ‘2’ is used hereafter to
35 reference the viscoelastic interlayer.
36
37

38
39 With regard to the shear behavior, the complex shear modulus, $G_2^*(\omega, T)$, is given by:
40
41

42
43
$$G_2^*(\omega, T) = G_2'(\omega, T) + i \cdot G_2''(\omega, T) = G_2'(\omega, T)(1 + i \cdot \eta_2(\omega, T)) \quad (3)$$

44
45
46

47 where $G'(\omega, T)$ and $G''(\omega, T)$ are the storage and the loss shear moduli, respectively.
48
49

50 Both the shear and tensile moduli can be related by means of the correspondence
51 principle [12, 13], introducing the corresponding complex viscoelastic properties, i.e.:
52
53
54
55
56
57
58
59
60
61
62
63
64
65

$$G_2^*(\omega, T) = \frac{3E_2^*(\omega, T) K_2^*(\omega, T)}{9K_2^*(\omega, T) - E_2^*(\omega, T)} \quad (4)$$

where $K_2^*(\omega, T)$ is the complex bulk modulus.

For the temperature dependence of the viscoelastic interlayer properties to be taken into account, a simply thermo-rheological behavior in the material is commonly assumed [14]. This enables a relation between time and temperature to be determined in linear viscoelastic materials using a Time-Temperature-Superposition (TTS) model such as the William-Landel-Ferry or Arrhenius equations [14, 15, 16]. Once the TTS model is fitted for a reference temperature, T_0 , i.e. the temperature used in the experimental tests, the moduli for the material to a different temperature, T_1 , can be estimated by shifting in time the moduli at temperature T_0 using a shift factor, $a_T(T_0, T_1)$, established from the material TTS model. A similar process can be followed in the frequency domain [14, 16].

To simplify the expressions in the text, we hereafter assume that the moduli for the interlayer have been previously calculated for the temperature of interest, so that only the frequency or time dependence of the viscoelastic interlayer will be taken into account in the expressions presented.

The mechanical performance of a viscoelastic material can be established by relaxation or creep tests in the time domain [14, 15]. The relaxation master curve, $E_2(t)$, is usually fitted with a generalized Maxwell model [16], which can be represented with a Prony series given by:

$$E_2(t) = E_2^\infty + \sum_{i=1}^n e_i e^{\left(-\frac{t}{\tau_i}\right)} \quad (5)$$

where e_i and τ_i are the Prony series coefficients to be estimated and E_∞ is the equilibrium modulus. The store and loss components of the complex modulus can be determined directly from the relaxation Prony series coefficients by:

$$E_2'(\omega) = E_2^\infty + \sum_{i=1}^n \frac{\tau_i^2 \omega^2 e_i}{1 + \tau_i^2 \omega^2} \quad (6)$$

and

$$E_2''(\omega) = E_2^\infty + \sum_{i=1}^n \frac{\tau_i \omega e_i}{1 + \tau_i^2 \omega^2} \quad (7)$$

Expressions similar to Eqs. (5, 6, and 7) can be used to determine the complex shear moduli from shear relaxation data.

The viscoelastic mechanical properties can also be determined by dynamic tests in the frequency domain [14, 15].

In this work, the complex shear modulus $G_2^*(\omega)$ and the complex tensile modulus $E_2^*(\omega)$ of the PVB interlayer at $T_0 = 20^\circ C$, shown in Figure 2, were considered [9]. The coefficients of the Willian-Landel-Ferry equation at $T_0 = 20^\circ C$ are $C_1 = 12.60$ and $C_2 = 74.46$.

2.2 Assumptions

The model proposed in this paper for the dynamic behaviour of laminated-glass plates considers the following assumptions:

- The glass layers exhibit linear-elastic behavior up to the first cracking and they carry both bending stress and shear stress. On the other hand, the contribution of the shear to the deflection is neglected. Thus, the glass behavior can be modeled by means of the Young modulus and the Poisson ratio [5- 6, 17- 28].

1
2
3
4 Although the glass behavior is assumed to be linear elastic, the entire section of
5 a laminated-glass element does not behave according to the Euler Bernoulli
6 assumptions (plane sections remain plane) and the normal stresses follow the
7 typical linear zigzag distribution through the thickness [25, 26, 28].
8
9

- 10
11
- 12 • There is no slipping between the elastic and viscoelastic layers at their
13 interfaces, i.e. the face layers and the interlayer are well bonded [17, 25-32].
14
 - 15 • The interlayer carries transverse shear stress and undergoes shear strain but the
16 longitudinal stresses are negligible. Thus, the behavior of the interlayer is
17 modeled by means of the shear modulus $G_2(t)$ in the time domain or $G_2^*(\omega)$ in
18 the frequency domain [5- 6, 17-28].
19
 - 20 • The ultimate strain of the interlayer is far greater than that of the glass plies. [17,
21 25- 29, 32- 34].
22
 - 23 • The interlayer exhibits a linear-viscoelastic behavior [18, 19, 20, 21, 22, 23, 24]
24 described by the shear modulus $G_2(t, T)$ or $G_2^*(\omega, T)$. This implies that all the
25 variables considered in the model (stiffness, deflections, stresses, effective
26 thicknesses, etc.) are time or frequency and temperature dependent.
27

28
29 However, some analytical models describe the viscoelastic behavior of the
30 interlayer by an elastic behavior with parameters that depend on the loading
31 duration and temperature [17, 25-27, 35];
32
33

- 34
- 35 • The normal stresses σ_z in the direction perpendicular to the plate can be
36 disregarded in both the glass plies and the interlayer. This assumption leads to
37 the idea that the three layers have the same transversal displacement, $w(x, \omega)$ or
38 $w(x, t)$ [27,29].
39
 - 40 • The deflections of the plate are minor, i.e. the effects of geometric non-linearity
41 are neglected [25, 26, 27, 28]
42
43
44
45
46
47
48
49

50
51 An extensive explanation of the assumptions considered in the analytical models for
52 laminated-glass elements can be seen in [17].
53
54
55
56
57
58
59
60
61
62
63
64
65

2.3 Analytical models for the static response of laminated-glass beams

In recent years, several models have been proposed for calculating deflections and stresses in laminated-glass beams under static loadings.

Asik and Tezcan [7] derived three coupled non-linear differential equations for analyzing laminated-glass beams which are valid for beams with different boundary conditions. An analytical solution to the differential equations is presented for the case of simply supported beams.

Ivanov [5] designed a simple mathematical model where the simple bending theory is applicable for the single glass layers and the effect of the shear of the PVB-interlayer is described by an additional differential equation.

Koutsawa and Daya [6] developed a mathematical model for the displacement, strain, and stress fields of laminated-glass beams on viscoelastic supports, which are modeled by two springs (rotational, K_R , and translational, K_T), on each extremity of the beam. The model is validated for the case of the simply supported beam, which is a particular case of the general model, assigning $K_R = 0$ and $K_T = \infty$.

Foraboschi [35] developed a mathematical model for determining the critical load, on laminated-glass beams subjected to compressive loads and provides a closed-form expression to calculate the critical load. The paper also provides rules in order to use laminated glass for compressive elements.

2.3.1 The model of Benninson et al.

Benninson et al. [1, 8] have proposed a model for the static calculation of laminated-glass elements based on a previous work by Wölfel [36], who proposed a model for a sandwich structure composed of three layers, the outer ones with considerable axial stiffness but negligible bending stiffness, while the inner layer can bear shear stress with only zero axial and flexural strength. Benninson et al. [1] and Calderone et al. [8] have extended Wölfel's approach specifically for the case of laminated glass. For the deflection of the laminated-glass beam, this model assumes a curve similar in type to that corresponding to a simply supported beam under uniformly distributed loading, and

these assumptions are valid for statically determined composite beams, for which the bending stiffness of the composite plies is negligible. According to Benninson et al. [1] and Calderone et al. [8], the stiffness of the entire laminated-glass beam is given by the equation:

$$EI(t)_S = E_1 I_T (1 + \Gamma_S(t) Y_1) \quad (8)$$

Where:

$$\Gamma_S(t) = \frac{1}{1 + \gamma \frac{E_1 H_1 H_2 H_3}{G_2(t) (H_1 + H_3) L^2}} \quad (9)$$

The subindex 's' indicates static, and γ is a scalar which depends on the boundary conditions [8]. The parameter $\Gamma_S(t)$ takes values in the range $0 \leq \Gamma_S(t) \leq 1$ corresponding $\Gamma_S = 0$ to the case of a layered beam ($G_2 = 0$) and $\Gamma_S = 1$ to a monolithic beam ($G_2 = \infty$).

This model was originally derived under the assumption that the glass plies have the same Young modulus, i.e. $E_1 = E_3$. However, it can easily be extended to hybrid laminated-glass beams with $E_1 \neq E_3$ by means of:

$$EI(t)_S = EI_T (1 + \Gamma_S(t) Y) \quad (10)$$

where

$$\Gamma_S(t) = \frac{1}{1 + \gamma \frac{E_1 H_1 H_2 E_3 H_3}{G_2(t) (E_1 H_1 + E_3 H_3) L^2}} \quad (11)$$

This model provides good results in simply supported beams but can provide only approximate results with other boundary conditions. However, it has the advantage that the equations are simple and easy to use.

2.3.2 The model of Galuppi and Royer Carfagni

Galuppi and Royer-Carfagni [3], based upon a variational approach, developed a model for calculating the deflection of laminated-glass beams under static loading that can be applied to a very wide range of boundary and loading conditions. The deflection of the beam is given by:

$$w(x, t) = -\frac{g(x)}{EI(t)_S} \quad (12)$$

where $g(x)$ is a shape function that takes the form of the elastic deflection of a monolithic beam having a constant cross-section under the same loading and boundary conditions as the laminated-glass beam, and $EI(t)_S$ is the bending stiffness of the laminated-glass beam given by:

$$EI(t)_S = \frac{E_1}{\frac{\eta_{S1}(t)}{I_{tot}} + \frac{1 - \eta_{S1}(t)}{I_1 + I_3}} \quad (13)$$

where

$$I_{tot} = I_1 + I_3 + \frac{H_1 H_3}{H_1 + H_3} H_0^2 = I_T(1 + Y_1) \quad (14)$$

and

$$\eta_{S1}(t) = \frac{1}{1 + \frac{I_1 + I_3}{I_{tot}} \frac{E_1}{G_2(t)} \frac{H_2 H_1 H_3}{H_1 + H_3} \psi_B} \quad (15)$$

The coefficient ψ_B depends on the geometry of the beam and on its boundary and loading conditions [3]. The values for the most practical cases are tabulated in [37].

If Eq. (14) is substituted in Eq. (15), it becomes:

$$\eta_{S1}(t) = \frac{1}{1 + \frac{E_1}{G_2(t)} \frac{H_2 H_1 H_3}{(H_1 + H_3)(1 + Y_1)}} \psi_B \quad (16)$$

The parameter $\eta_{S1}(t)$ takes values in the range $0 \leq \eta_{S1}(t) \leq 1$ corresponding $\eta_{S1} = 0$ to the case of a layered beam and $\eta_{S1} = 1$ to a monolithic beam.

The identification of Eq. (8) and Eq. (15) gives:

$$\psi_B = \gamma/L^2 \quad (17)$$

This model can also be extended to hybrid laminated-glass beams ($E_1 \neq E_3$) with the expressions:

$$EI(t)_S = \frac{1}{\frac{\eta_S(t)}{EI_T(1 + Y)} + \frac{1 - \eta_S(t)}{EI_T}} \quad (18)$$

where

$$\eta_S(t) = \frac{1}{1 + \frac{E_1 H_1 H_2 E_3 H_3}{(1 + Y) G_2(t) (E_1 H_1 + E_3 H_3)}} \psi_B \quad (19)$$

2.4 Analytical models for the static response of laminated-glass plates

Foraboschi [17] has proposed a model for the static response of laminated-glass plates with thin and soft interlayer which consists of a system of three analytical equations, derived from the Kirchhoff–Love assumptions for thin plates with small deflections, and a solution for a rectangular simply supported plate under uniformly distributed static loading is provided. However, the model can be applied to different shapes,

1
2
3
4 boundary conditions, and loadings, using proper boundary conditions and a
5 mathematical form of the series for the loading and the solution.
6

7
8 An analytical model for a sandwich plate with a soft interlayer of any thickness was
9 derived by Foraboschi [26]. An exact solution for laminated-glass plates with an
10 interlayer of any thickness and any transverse elasticity modulus was proposed by
11 Foraboschi [29].
12
13
14

15
16 In the models [17, 26 and 29] the viscoelastic behaviour of the interlayer is modeled in a
17 linear elastic manner by means of the shear modulus G_2 provided that it is related to the
18 temperature and duration of the loading.
19
20
21

22 23 *2.4.1 The model of Galuppi and Royer Carfagni.*

24 Galuppi and Royer-Carfagni [4] have extended the model for beams [3] to the two-
25 dimensional case of a rectangular laminated-glass plates under uniform pressure with
26 different boundary configurations at the borders. They have considered the deflection of
27 the plate as:
28
29
30

$$31 \quad w(x, y, t) = -\frac{g(x, y)}{D(t)_S} \quad (20)$$

32
33 where $g(x, y)$ is a shape function that takes the form of the elastic deflection of a
34 monolithic plate with constant cross-section under the same loading and boundary
35 conditions. The shape function $g(x, y)$ is approximated by the first term of the series
36 expansion for the deflection surface of a monolithic plate. The flexural stiffness $D(t)_S$
37 is expressed as:
38
39
40
41
42
43
44
45
46
47
48
49

$$50 \quad D(t)_S = \frac{1}{\left(\frac{\eta_{SP}(t)}{D_{tot}} + \frac{1 - \eta_{SP}(t)}{D_1 + D_3}\right)} \quad (21)$$

51
52 where:
53
54
55
56
57
58
59
60
61
62
63
64
65

$$D_{tot} = D_1 + D_3 + \frac{12 D_1 D_3}{D_1 H_3^2 + D_3 H_1^2} H_0^2 \quad (22)$$

and

$$\eta_{sp}(t) = \frac{1}{1 + \frac{H_2(D_1 + D_3)}{G_2(t)D_{tot}} \cdot \frac{12 D_1 D_3}{D_1 H_3^2 + D_3 H_1^2} \psi_P} \quad (23)$$

and the subindex “p” indicates plate.

Again, the coefficient ψ_P depends on the geometry of the plate and on its boundary and loading conditions and their values for the most common practical cases are tabulated in [37].

Eq. (21) can also be expressed as:

$$D(t)_s = \frac{1}{\left(\frac{\eta_{sp}(t)}{(D_1 + D_3)(1 + Y_P)} + \frac{1 - \eta_{sp}(t)}{D_1 + D_3} \right)} \quad (24)$$

where

$$Y_P = \frac{H_0^2 \frac{E_1 H_1}{(1 - \nu_1^2)} \frac{E_3 H_3}{(1 - \nu_3^2)}}{(D_1 + D_3) \left(\frac{E_1 H_1}{(1 - \nu_1^2)} + \frac{E_3 H_3}{(1 - \nu_3^2)} \right)} \quad (25)$$

If $E_1 = E_3$ and $\nu_1 = \nu_3$ it is inferred from eq. (25) that $Y_P = Y = Y_1$.

2.4 Analytical models for the dynamic response of laminated-glass beams

In the 1960s and 70s, several models were proposed about the dynamic flexural vibration of sandwich beams with viscoelastic core. Ross, Ungar, and Kerwin, the first to study the flexural vibration of a sandwich configuration [18, 19], proposed an effective complex flexural stiffness which can be used to determine the modal parameters of a sandwich beam using the equations and the wavenumbers corresponding to an Euler-Bernoulli beam. DiTaranto [20, 21] and Mead and Markus [22, 23] demonstrated that the flexural motion of a sandwich beam is governed by a sixth-order linear homogeneous differential equation. Rao derived a similar equation of motion using Hamilton's principle [24].

2.4.1 The model of Mead and Markus (M&M)

Mead and Markus [23, 24] formulated a sixth-order differential equation that governs the flexural wave motion of a three-layered constrained-layer damping beam when it vibrates freely at frequency ω , which is given by:

$$EI_T (w^{VI}(x) - g_M^*(\omega) (1 + Y) w^{IV}(x)) - \omega^2 \bar{m} (w^{II}(x) - g_M^*(\omega) w(x)) = 0 \quad (26)$$

where the term \bar{m} is the mass per unit area i.e.:

$$\bar{m} = (\rho_1 H_1 + \rho_2 H_2 + \rho_3 H_3) \quad (27)$$

g_M^* is a shear parameter given by:

$$g_M^*(\omega) = \frac{G_2^*(\omega) L^2 (E_1 H_1 + E_3 H_3)}{H_2 E_1 H_1 E_3 H_3} \quad (28)$$

and the superindex “*” indicates complex.

Eq. (26) yields the following polynomial equation:

$$(k_M^* L)^6 - g_M^*(\omega)(1 + Y)(k_M^* L)^4 - \Omega^{*2}(k_M^* L)^2 + \Omega^{*2} g_M^* = 0 \quad (29)$$

Where $k_M^* = k_R + i \cdot k_I$ is the complex wavenumber and Ω^* is a non-dimensional complex frequency defined by [21- 24]:

$$\Omega^{*2} = \frac{\omega^{*2} \bar{m} L^4}{EI_T} \quad (30)$$

The complex Eq. (29), together with the sixth-order characteristic determinant formed using appropriate boundary conditions in Eq. (26), provides the three complex pairs of k_M^* , the complex mode shapes and the complex non-dimensional resonance frequency Ω^* [22, 23]. If Eq. (29) is substituted in Eq. (30) the natural frequency, ω , and loss factor, η , are given by :

$$\omega^{*2} = \omega^2(1 + i \cdot \eta) = \frac{k_M^{*4}}{\bar{m}} EI_T \left(\frac{(k_M^* L)^2 - g_M^*(\omega)(1 + Y)}{(k_M^* L)^2 - g_M^*(\omega)} \right) \quad (31)$$

2.4.2 The model of Ross, Kerwin and Ungar (RKU)

Ross, Ungar, and Kerwin [18, 19] developed a model for the flexural vibrations of sandwich elements considering the beam simply supported and assuming a flexural deformation spatially sinusoidal in shape. With these assumptions the equation of motion is formulated as:

$$EI^*(\omega) w(x, t)^{IV} + \bar{m} \ddot{w}(x, t) = 0 \quad (32)$$

where $EI^*(\omega)$ is an effective complex flexural stiffness given by:

$$\begin{aligned}
EI^*(\omega) &= EI_T \left(1 + \frac{Y g_R^*(\omega) \left(1 + \frac{E_3 H_3}{E_1 H_1}\right)}{1 + g_R^*(\omega) \left(1 + \frac{E_3 H_3}{E_1 H_1}\right)} \right) \\
&= EI_T \left(1 + \frac{Y}{1 + \frac{E_1 H_1}{g_R^*(\omega) (E_1 H_1 + E_3 H_3)}} \right)
\end{aligned} \tag{33}$$

$g_R^*(\omega)$ is a shear parameter:

$$g_R^*(\omega) = \frac{G_2^*(\omega)}{E_3 H_3 H_2 k_l^2} \tag{34}$$

and k_l is the wavenumber.

The complex natural frequencies are estimated with the expression:

$$\omega^{*2} = \omega^2 (1 + i \cdot \eta) = k_l^4 \frac{EI^*(\omega)}{\bar{m}} \tag{35}$$

where \bar{m} is the mass per unit length (Eq. 27).

2.5 Analytical models for the dynamic response of laminated-glass plates

Some models have been proposed in the past for sandwich plates with elastic faces and elastic core. Wang [38] has derived an exact relationship between the natural frequencies of a simply supported rectangular sandwich plate and those corresponding to a monolithic Kirchhoff plate with the same geometry and boundary conditions. It is assumed in the model that the variation of the in-plane displacement through the thickness is linear and that the behaviour of faces and core is linear elastic. Thus, exact

sandwich plate solutions can be arrived at if the solution of the Kirchhoff plate is also exact. Modification factors can be used in the formulas to consider other boundary conditions. However, the damping cannot be predicted with this model.

2.5.1 The model of Nashif et al.

The natural frequencies of a rectangular monolithic plate can be estimated by means of the equation [39]:

$$\omega^2 = K_I^4 \frac{D}{\rho H} \quad (36)$$

where k_I is the wave number, ρ the mass density, H the thickness of the plate and D is the flexural stiffness given by:

$$D = \frac{EH^3}{12(1 - \nu^2)} \quad (37)$$

with ν being the Poisson ratio.

Nashif et al. [40] proposed to extend the RKU model for beams (Section 2.4.2) to the two-dimensional case of rectangular laminated-glass plates. Under the same assumptions as those considered for beams, the natural frequencies and loss factor of a rectangular laminated-glass plate can be predicted with:

$$\omega^2(1 + i\eta) = k_I^4 \frac{D_{Nas}^*(\omega)}{(\rho H)_{eq}} \quad (38)$$

Where $(\rho H)_{eq}$ is the mass per unit area:

1
2
3
4
5
6
7
8
9
10
11
12
13
14
15
16
17
18
19
20
21
22
23
24
25
26
27
28
29
30
31
32
33
34
35
36
37
38
39
40
41
42
43
44
45
46
47
48
49
50
51
52
53
54
55
56
57
58
59
60
61
62
63
64
65

$$(\rho H)_{eq} = \rho_1 H_1 + \rho_2 H_2 + \rho_3 H_3 \quad (39)$$

$D_{Nas}^*(\omega)$ is the complex effective stiffness which is expressed as:

$$D_{Nas}^*(\omega) = \frac{EI^*(\omega)}{(1 - \nu^{*2})} \quad (40)$$

And the subindex “ Nas ” refers to Nashif.

In Eq. (40) $EI^*(\omega)$ is the effective stiffness given by Eq. (33) and ν^* is the complex effective Poisson ratio but no expressions for ν^* are proposed by the authors [40].

2.6 Effective thickness

The concept of effective thickness for simplifying the calculations of laminated-glass elements under static loading was firstly proposed by Benninson et al. [1,8]. The static deflection-effective thickness is defined as the (constant) thickness of a monolithic glass with the same width and length, which gives the same displacement as does the laminated-glass beam under the same loading [1, 8]. As the behavior of the laminated-glass elements are time and temperature dependent, an effective thickness has to be determined for each time and temperature.

The effective deflection thickness is derived from the stiffness of the laminated-glass beam and consequently the stiffness given by Eqs. (10) and (18) can be considered effective stiffness. This also means that an effective Young modulus can easily be derived using the same technique which, on the other hand, is more appealing for use in numerical and analytical models —that is, the monolithic model has constant thickness whereas a time- or frequency-dependent Young modulus is defined.

The same concept can be used to determine stresses in laminated-glass elements with the particularity that different effective thicknesses need to be determined for each of the glass plies at each section. If the goal is the maximum stress, the stress-effective

1
2
3
4 thickness of a laminated-glass beam ply is defined as the (constant) thickness of a
5 monolithic glass beam that, under the same boundary and load conditions of the
6 problem at hand, presents the same maximum stress [1, 3, 8]. Thus, an effective
7 thickness has to be determined for each of the glass layers.
8
9

10
11
12 If we are interested in the stress distribution (the typical zigzag distribution of normal
13 stresses through the thickness) in the glass layers, we need to estimate two stress-
14 effective thicknesses for each glass layer: one at the top and another one at the bottom
15 of each layer. This means that the stress effective thickness is useful to estimate the
16 maximum stresses, but four different stress effective thicknesses have to be calculated
17 to determine the complete stress distribution.
18
19
20
21
22

23
24 As for the dynamic effective thickness for estimating the modal parameters, only one
25 effective thickness (frequency and temperature dependent) is needed to estimate the
26 natural frequencies and loss factors corresponding to all the modes [9]. With respect to
27 the mode shapes, they are assumed to be equal to those of the monolithic beam with the
28 same boundary conditions.
29
30
31
32

33
34 Due to the assumptions considered in the derivation of the effective-thickness equations
35 [3, 4, 9] they cannot provide exact results. However, the numerical simulations and the
36 experimental results demonstrate that quite accurate results can be reached with this
37 technique [3, 4, 9].
38
39
40

41 *2.6.1 Static deflection effective thickness and deflection effective Young modulus*

42

43
44 The deflection effective thickness for laminated-glass beams can be determined by
45 identifying the stiffness of a monolithic beam with Young modulus E_i and thickness
46 H_{eff} and the stiffness given by Eqs. (10, 18), i.e.:

$$47 \frac{E_i H_{effS}^3(t)}{12} = EI(t)_S \quad (41)$$

48
49
50
51
52
53
54
55

56 where the subindex “ $_{effS}$ ” indicates effectives for static loading .
57
58
59
60
61
62
63
64
65

1
2
3
4 On the other hand, the effective Young modulus is derived from:
5
6

$$\frac{E_{eff}(t)H^3}{12} = EI(t)_S \quad (42)$$

7
8
9
10
11
12

13 Where H is the thickness of the monolithic beam. In order for the effective Young
14 modulus to be close to that corresponding to the glass, the thickness H should be taken
15 as:
16
17

$$H = H_1 + H_2 + H_3 \quad (43)$$

18
19
20
21
22
23
24

25 The equations of the effective thickness and effective Young modulus for beams are
26 shown in Table 1. If $E_1 = E_3$, there is a unique effective thickness whereas two
27 different effective thicknesses have to be defined if $E_1 \neq E_3$ —that is, the effective
28 thickness differs depending on whether the monolithic model has Young modules E_1 or
29 E_3 . In any case, the effective Young modulus is unique.
30
31
32
33

34 In case of plates, three parameters are needed to define the stiffness of a plate
35 (thickness, Young modulus and Poisson ratio). The effective thickness with Young
36 modulus E_i and Poisson ratio ν_i is derived from:
37
38
39
40
41

$$\frac{E_i H_{effS}^3(t)}{12(1 - \nu_i^2)} = D(t)_S \quad (44)$$

42
43
44
45
46
47

48 If we use a constant thickness to determine an effective Young modulus, two parameters
49 still remain unknown: the Young modulus and the Poisson ratio. To get reasonable
50 values for E_{eff} , we can take Poisson ratios equal to that corresponding to the glass, i.e.
51
52
53
54
55
56
57
58
59
60
61
62
63
64
65

$$\frac{E_{eff}(t)H^3}{12(1 - \nu_{eff}^2(t))} = D(t)_S \quad (45)$$

where $\nu_{eff}(t) = \nu_1$ or $\nu_{eff}(t) = \nu_3$.

The equations of the effective thickness and effective Young modulus for plates are shown in Table 1.

2.7 Dynamic effective thickness for laminated-glass beams

Aenlle and Pelayo [9] demonstrated that the RKU model can be considered a particular case of M&M model when $k_R = 0$, *i. e.*, Eq. (31) and Eq. (35) provide the same modal parameters when $k_R = 0$. On the other hand, the RKU model provides reasonably accurate results when k_R is small. Thus, the effective stiffness given by Eq. (33) can be used together with the Eq. (35) to predict accurately the modal parameters of laminated-glass beams when k_R is small. Moreover, a dynamic effective stiffness was derived from Eq. (33), which is given by:

$$EI^*(\omega) = EI_T \left(1 + \frac{Y}{1 + \frac{E_1 H_1}{g_R^*(\omega)(E_1 H_1 + E_3 H_3)}} \right) \quad (46)$$

which can also be expressed as:

$$EI^*(\omega) = EI_T \left(1 + \frac{Y}{1 + \frac{E_1 H_1 E_3 H_3 k_l^2}{G_2^*(\omega)(E_1 H_1 + E_3 H_3)}} \right) \quad (47)$$

The dynamic effective thickness and the effective Young modulus are estimated using the same methodology as that used in statics, and the results are shown in Table 2.

Using the same format as the effective stiffness for statics proposed by Galuppi et al., Eq. (46) can be expressed as:

$$EI^*(\omega) = \frac{1}{\frac{\eta_d(\omega)}{EI_T(1+Y)} + \frac{1-\eta_d(\omega)}{EI_T}} \quad (48)$$

where

$$\begin{aligned} \eta_d(\omega) &= \frac{1}{1 + \frac{E_1 H_1}{g_R^*(\omega)(E_1 H_1 + E_3 H_3)(1+Y)}} \\ &= \frac{1}{1 + \frac{E_1 H_1 H_2 E_3 H_3 k_I^2}{G_2^*(\omega)(E_1 H_1 + E_3 H_3)(1+Y)}} \end{aligned} \quad (49)$$

3 A MODEL FOR THE DYNAMIC BEHAVIOUR OF LAMINATED-GLASS PLATES

In this section, we extend the model of Ross, Kerwin and Ungar to rectangular laminated-glass plates. Furthermore, a dynamic effective thickness and a dynamic effective Young modulus are derived to estimate the modal parameters in laminated-glass plates. The method is based on the relationship that exists between the static $EI(t)_S$ and the dynamic $EI^*(t)$ stiffness in beams.

3.1 Relation between $EI(t)_S$ and $EI^*(\omega)$ in beams.

From Eqs. (18) and (48) it is inferred that the only difference between them (apart from the time t and the frequency ω) are the parameters ψ_B and k_I .

In Galuppi and Royer Carfagni [3], it is proposed to calculate the parameter ψ_B (Eq. (17)) by means of:

$$\psi_B = \frac{\int_{-L/2}^{L/2} g''(x)^2 dx}{\int_{-L/2}^{L/2} g'(x)^2 dx} ; \quad -\frac{L}{2} \leq x \leq L/2 \quad (50)$$

Where $g(x)$ is a function equal in shape to the bending deflection of an elastic monolithic beam with constant cross-section under the same loading and boundary conditions as the problem at hand.

On the other hand, the critical load of an elastic monolithic beam with constant cross-section and stiffness EI , using the Rayleigh Ritz method with an approximate deflection curve $g(x)$, is given by:

$$N_{crit} = \frac{\pi^2 EI}{(L_{eff})^2} = \frac{\int_{-L/2}^{L/2} EI g''(x)^2 dx}{\int_{-L/2}^{L/2} g'(x)^2 dx} \quad (51)$$

where L_{eff} is the effective length. Identifying Eqs. (50 and (51) we get:

$$L_{eff} = \frac{\pi}{\sqrt{\psi_B}} \quad (52)$$

This means that the parameter ψ_B is related to the effective length $L_{eff} = \beta L$, β being the buckling ratio of the beam, i.e. with the semi-wavelength of the deflection curve (distance between the inflection points). The result of Eq. (52) can be checked with the values of ψ_B provided in Table 1 of [37].

On the other hand, the wavenumber k_I is related to the wavelength λ by means of:

$$\lambda = 2\pi/k_I \quad (53)$$

Thus, the wavenumber k_I plays in dynamics the same role as parameter $\sqrt{\psi_B}$ in statics or, alternatively, the effective length L_{eff} (semi-wavelength of the deflection curve) plays the same role in statics as the semi-wavelength $\frac{\lambda}{2}$ in dynamics. This also means that the dynamic stiffness can be determined from the static stiffness changing time (t) per frequency (ω) and $\sqrt{\psi_B}$ per k_I .

Therefore, $EI(t)_S$ depends on the boundary conditions and its effect can be described with the parameter ψ_B or, alternatively, with the effective length of the buckling-mode shape. With respect to $EI^*(\omega)$, the effect of the boundary conditions is considered with the wavenumber k_I . For a simply supported beam, the parameters ψ_B and k_I are given by:

$$\psi_B = k_I^2 = \frac{n^2\pi}{L^2} \quad (52)$$

where n is an integer indicating the order of the mode. The relation given by Eq. (52) is expected because in the models developed in [3] and [9] it is assumed that the static and the dynamic deflection shapes of laminated-glass beams are equal to those of the monolithic beams.

32. Extension to rectangular plates.

In this section, the relation between the static and the dynamic stiffness derived for beams can be extended to rectangular plates. In [4] the parameter ψ_P for plates, is given by:

$$\psi_P = \frac{\int_{\Omega} \left[\left(\frac{\partial^2 g(x,y)}{\partial x^2} + \frac{\partial^2 g(x,y)}{\partial y^2} \right)^2 - 2(1-\nu) \left(\frac{\partial^2 g(x,y)}{\partial x^2} \frac{\partial^2 g(x,y)}{\partial y^2} - \left(\frac{\partial^2 g(x,y)}{\partial x \partial y} \right)^2 \right) \right] dx dy}{\int_{\Omega} \left[\left(\frac{\partial g(x,y)}{\partial x} \right)^2 + \left(\frac{\partial g(x,y)}{\partial y} \right)^2 \right] dx dy} \quad (55)$$

Where Ω is the domain of the plate and $g(x, y)$ is a function equal in shape to the bending deflection of an elastic monolithic plate with constant cross-section under the same loading and boundary conditions of the problem at hand.

On the other hand, the critical loading of a rectangular plate subject to normal loadings $N_x = N, N_y = N$ and $N_{xy} = 0$ using the Rayleigh-Ritz method with an approximate deflection surface $g(x, y)$ is given by:

$$N_{crit} = D \frac{\int_{\Omega} \left[\left(\frac{\partial^2 g(x, y)}{\partial x^2} + \frac{\partial^2 g(x, y)}{\partial y^2} \right)^2 - 2(1 - \nu) \left(\frac{\partial^2 g(x, y)}{\partial x^2} \frac{\partial^2 g(x, y)}{\partial y^2} - \left(\frac{\partial^2 g(x, y)}{\partial x \partial y} \right)^2 \right) \right] dx dy}{\int_{\Omega} \left[\left(\frac{\partial g(x, y)}{\partial x} \right)^2 + \left(\frac{\partial g(x, y)}{\partial y} \right)^2 \right] dx dy} \quad (56)$$

Identifying Eqs. (55) and (56), the critical load is given by:

$$N_{crit} = D \psi_P \quad (57)$$

For the particular case of a simply supported plate:

$$N_{crit} = D \pi^2 \left(\left(\frac{m}{a} \right)^2 + \left(\frac{n}{b} \right)^2 \right) \quad (58)$$

Where m and n are the half-waves of buckling in x and y directions, respectively, and a and b are the dimensions of the plate in the same directions.

From Eqs. (57) and (58) it is derived that for this particular boundary condition:

$$\psi_P = \pi^2 \left(\left(\frac{m}{a} \right)^2 + \left(\frac{n}{b} \right)^2 \right) \quad (59)$$

With respect to the wavenumbers of a simply supported plate, they are given by:

$$k_I^2 = \pi^2 \left(\left(\frac{m}{a} \right)^2 + \left(\frac{n}{b} \right)^2 \right) \quad (60)$$

i.e. $\psi_P = k_I^2$, as in monolithic plates.

Thus, the parameter ψ_P is related, as in beams, to the dimension of the half-waves that the plates buckle into, i.e. the stiffness $D(t)_S$ depends on the boundary conditions. A dynamic stiffness $D^*(\omega)$ can be derived from the static stiffness $D(t)_S$ (Eq. (21)) of the Galuppi and Royer Carfagni model by extending to plates the relationship between the static and the dynamic stiffnesses derived for beams, i.e. changing time (t) per frequency (ω) and ψ_P per k_I^2 . With this assumption, the dynamic stiffness $D^*(\omega)$ is expressed as:

$$D^*(\omega) = \frac{1}{\left(\frac{\eta_{dP}(\omega, T)}{(D_1 + D_3)(1 + Y_P)} + \frac{1 - \eta_{dP}(\omega)}{D_1 + D_3} \right)} \quad (61)$$

where the parameter $\eta_{dP}(\omega)$ is given by:

$$\eta_{dP}(\omega) = \frac{1}{1 + \frac{(D_1 + D_3) H_2}{G_2^*(\omega) D_{tot}} \frac{12 D_1 D_3}{(D_1 H_3^2 + D_3 H_1^2)} k_I^2} \quad (62)$$

or alternatively

$$\eta_{dP}(\omega) = \frac{1}{1 + \frac{\frac{E_1 H_1}{(1 - \nu_1^2)} H_2 \frac{E_3 H_3}{(1 - \nu_3^2)} k_I^2}{G_2^*(\omega) \left(\frac{E_1 H_1}{(1 - \nu_1^2)} + \frac{E_3 H_3}{(1 - \nu_3^2)} \right) (1 + Y_P)}} \quad (63)$$

The stiffness given by Eq. (61) can be considered an effective stiffness for laminated-glass plates—that is, a monolithic plate model with stiffness $D^*(\omega)$ will give the same

modal parameters as the laminated-glass plate. Finally, the natural frequencies and loss factors are found by means of:

$$\omega^2(1 + i\eta) = k_I^4 \frac{D^*(\omega)}{(\rho H)_{eq}} \quad (64)$$

With respect to the mode shapes, it has been validated by experimental tests in laminated-glass elements [41] and finite element models [42, 43] that the mode shapes of laminated-glass beams and plates present a very good correlation with those corresponding to a monolithic element with the same dimensions and supports as the laminated-glass element. This assumption has also been considered in this paper.

3.3 Dynamic effective thickness for laminated-glass plates

The dynamic effective thickness with Young modulus E_i and Poisson ratio ν_i is derived from:

$$\frac{E_i H_{ieff}(\omega)^3}{12(1 - \nu_i^2)} = D^*(\omega) \quad (65)$$

From Eqs. (61) and (65) it is inferred that the dynamic effective thicknesses are given by:

$$H_{1eff}(\omega) = \sqrt[3]{\frac{12(D_1 + D_3)(1 + Y_P)}{E_1(1 - \nu_1^2) \left(1 + Y_P (1 - \eta_{dp}(\omega))\right)}} \quad (66)$$

and

$$H_{3eff}(\omega) = \sqrt[3]{\frac{12(D_1 + D_3)(1 + Y_P)}{E_3(1 - \nu_3^2) \left(1 + Y_P (1 - \eta_{dp}(\omega))\right)}} \quad (67)$$

whereas the effective Young modulus is expressed as:

$$E_{eff}(\omega) = \frac{12(1 - \nu_{eff}^2)(D_1 + D_3)(1 + Y_P)}{H^3(1 + Y_P(1 - \eta_{dP}(\omega)))} \quad (68)$$

where $\nu_{eff} = \nu_1$ or $\nu_{eff} = \nu_1$. If $E_1 = E_3$ and $\nu_1 = \nu_3$ Eq. (63) simplifies to:

$$\eta_{dP}(\omega) = \frac{1}{1 + \frac{E_1 H_1 H_2 H_3 k_l^2}{G_2^*(\omega)(H_1 + H_3)(1 + Y)(1 - \nu_1^2)}} \quad (69)$$

Eqs. (66) and (67) to:

$$H_{1eff}(\omega) = H_{3eff}(\omega) = \sqrt[3]{\frac{(H_1^3 + H_3^3)(1 + Y)}{1 + Y(1 - \eta_{dP}(\omega))}} \quad (70)$$

and Eq. (68) to:

$$E_{eff}(\omega) = \frac{(H_1^3 + H_3^3)(1 + Y)}{H^3(1 + Y(1 - \eta_{dP}(\omega)))} \quad (71)$$

3. 4 METHODOLOGY

3.4.1 Methodology I. Stiffness Method

This methodology is recommended when the wavenumbers k_I are known from the literature (see e.g. [39]) and it is shown schematically in Fig 3. The technique consists of the following steps:

1. To estimate an initial natural frequency ω_0 . The laminated-glass plates have two border lines [2] (the layered limit and the monolithic limit) so that the natural frequency has to be within the range:

$$k_I^4 \frac{D_{layered}}{(\rho H)_{eq}} \leq \omega_0 \leq k_I^4 \frac{D_{monolithic}}{(\rho H)_{eq}} \quad (72)$$

The average of both limits can be taken as the initial natural frequency, so that:

$$\begin{aligned} \omega_0^2 &= \frac{\frac{k_I^4}{(\rho H)_{eq}} (D_{monolithic} + D_{layered})}{2} \\ &= \frac{k_I^4 D_{monolithic}}{(\rho H)_{eq}} \left(1 + \frac{H_1^3 + H_3^3}{(H_1 + H_2 + H_3)^3} \right) \end{aligned} \quad (73)$$

2. To calculate $\eta_{dp}(\omega)$ with Eq. (63). The wavenumbers corresponding to each mode are needed in Eq. (63) and those corresponding to a monolithic plate with the same boundary conditions can be used with reasonable accuracy. They can be taken from the literature [39] for the most common cases.
3. To calculate $D^*(\omega)$ with Eq. (61).
4. To calculate the natural frequency ω and the loss factor η with Eq. (64).
5. To repeat steps 2, 3, and 4 up to convergence (the error between the frequency ω in steps 2 and 3 and the frequency ω in step 4 is small)

In these steps, $\omega = \omega_0$ is considered in the first iteration.

3.4.2 Methodology II: effective thickness

This methodology, based on the dynamic effective thickness concept is recommended when the wavenumbers corresponding to the boundary conditions are not known from the literature. The procedure, shown schematically in Fig 4, is the following:

1. To assemble a monolithic FE model with the same dimensions as the laminated-glass plate, thickness $H = H_1 + H_2 + H_3$, material properties E_1, ν_1 and density:

$$\rho_{eq} = \frac{\rho_1 H_1 + \rho_2 H_2 + \rho_3 H_3}{H_1 + H_2 + H_3} \quad (74)$$

Alternatively, material properties E_3, ν_3 can be used if H_{3eff} is considered in Eq. (65).

This monolithic model will provide us the following information:

- The mode shapes of the laminated-glass plate.
- The wavenumbers k_I needed in Eqs. (63) and (65). They can be estimated from the natural frequencies of the finite-element monolithic model using the equation:

$$\omega_{mon}^2 = k_I^4 \frac{E_1 H^3}{12(1 - \nu_1^2) \rho_{eq} H} \quad (75)$$

where the wavenumbers are the only unknowns.

- An initial natural frequency ω_0 which can be estimated with the equation:

$$\omega_0^2 = \frac{\frac{12 k_I^4}{(1 - \nu_1^2)(\rho H)_{eq}} ((H_1 + H_2 + H_3)^3 + (H_1^3 + H_3^3))}{2} \quad (76)$$

which is the average between the layered and the monolithic limit.

2. To calculate $\eta_{dp}(\omega)$ with Eq. (63).
3. To calculate the effective thickness, $H_{1eff}(\omega)$ with Eq. (64).
4. To calculate the natural frequency and the loss factors with:

$$\omega^2(1 + i\eta) = \omega_{mon}^2 \frac{H_{1eff}(\omega)^3}{H^3} \quad (77)$$

5. To repeat steps 2, 3, and 4 up to convergence (the error between the frequency ω in steps 2 and 3 and the frequency ω in step 4 is small).

Once again, in these steps, $\omega = \omega_0$ is considered in the first iteration.

4 EXPERIMENTAL TESTS

4.1 Laminated-glass plate

A rectangular laminated-glass plate 1400 x 1000 mm and thickness $H_1 = 7.82$ mm, $H_2 = 0.76$ mm, $H_3 = 7.828$ mm, pinned supported at the four corners, were tested using operational modal analysis (OMA), with the temperature being $T = 20.5$ °C (Fig 5). The interlayer was made of PVB whereas the faces were made of annealed glass. To study the effect of the supports on the damping, we made the experimental tests using two different supports. The first test was performed using four wooden balls 50 mm in diameter whereas four smaller steel balls (8 mm in diameter) were used in the second test (see Fig. 6).

Operational Modal Analysis is a technique that allows us to estimate the model parameters (natural frequencies, mode shapes, and damping ratios) without knowing and/or controlling the input excitation [44]. OMA is a Multiple Input Multiple Output (MIMO) technique; that is, the technique is able to estimate closely space modes and even repeated modes with a high degree of accuracy. The testing is easier than the traditional modal analysis because there is no need for an exciter (vibration shaker, impact hammer, etc.). The ideal force for operational modal analysis is stationary white noise. In practice, we need only to make sure that the loading is reasonably random in time and space. The excitation produced in this way will be a good approximation of a multivariate white-noise stochastic process. Other important features are that the estimated modes are based on true boundary conditions and the actual ambient excitation sources. When operational modal analysis is applied to structures located in the labs or places where the magnitude of the natural loads is relatively low, artificial devices must be used in order to reach a reasonable load magnitude which, additionally, must be multiple-input and stationary broad banded [45]. A procedure to approximate to this loading consists of applying many hits over a large part of the structure.

The plate was excited by applying many small hits with an impact hammer on the plate surface randomly in time and space. The responses of the plate were measured using 16 accelerometers with a sensitivity of 100 mv/g, uniformly distributed (Figure 5). The responses were recorded for approximately 5 min with a sampling frequency of 1632

1
2
3
4 Hz and using a 16 channel (4xNI9234) Compact DAQ acquisition system by National
5 instruments. The first 8 modes were identified by OMA and the modal parameters of the
6 plate were estimated using both the frequency-domain decomposition (FDD) [44] and
7 the stochastic subspace iteration method (SSI) [46]. The two techniques provide similar
8 results, and therefore only the modal parameters estimated with the FDD technique are
9 shown in Table 3 for both types of supports.
10
11
12
13
14

15 *4.2 Laminated-glass beam*

16
17 To validate the model for different boundary conditions and also at different
18 temperatures, we estimated the modal parameters of a free-free laminated-glass beam,
19 with the following geometrical data: $L = 1$ m, $H_1 = 3.75$ mm, $H_2 = 0.38$ mm, $H_3 =$
20 7.90 mm, $b = 0.1$ m, using OMA. The faces were also annealed glass whereas the core
21 was PVB.
22
23
24
25
26
27

28 The tests were performed in a climate chamber at temperatures: 12 °C, 20 °C, 25 °C,
29 30 °C, 35 °C, 40 °C, and 45 °C. The responses of the beams were measured using 8
30 accelerometers with a sensitivity of 100 mv/g, uniformly distributed (Figure 7) and an
31 8-channel National Instruments digital card. The arrows in Fig. 7 show the location and
32 the direction of the sensors. The beam was excited by applying many hits along the
33 beam, random in time and space, and the responses were recorded for approximately 5
34 min using a sampling frequency of 2132 Hz.
35
36
37
38
39
40

41 The modal parameters were estimated using both frequency-domain decomposition [44]
42 and the stochastic subspace iteration method (SSI) [46]. The modal parameters
43 corresponding to the first three modes, estimated with the FDD technique, are presented
44 in Table 4.
45
46
47
48

49 5 VALIDATION OF THE MODEL

50 *5.1 Laminated-glass plate*

51
52 The modal parameters of the plate described in the former section were also predicted
53 using the dynamic effective concept. A Young modulus $E_1 = 72000$ MPa, Poisson
54
55
56
57
58
59
60
61
62
63
64
65

ratio $\nu_1 = 0.22$ and density $\rho_1 = 2500 \text{ kg/m}^3$ were considered for the glass [9]. With regard to the core of the beam, made of polyvinyl butyral (PVB), a density $\rho_2 = 1030 \text{ kg/m}^3$ and the complex shear modulus $G_2^*(\omega)$ indicated in Figure 2 were considered [9].

In Section 3 two different methodologies were proposed to estimate the modal parameters of laminated-glass plate, both providing the same results. In this paper, methodology II, which considers the dynamic effective thickness concept, was used (Eqs. (66) and (77)).

A FEM of a rectangular monolithic glass plate $1400 \times 1000 \text{ mm}^2$, thickness $H = H_1 + H_2 + H_3 = 16.40 \text{ mm}$, pin supported at the corners and material properties corresponding to the glass (E_1, ρ_1, ν_1), was assembled in ABAQUS and the natural frequencies ω_{FEM} of the first 8 modes were extracted. The wavenumbers corresponding to this monolithic model were calculated from the equation:

$$\omega_{FEM}^2 = k_I^4 \frac{E_1 \frac{(H_1 + H_2 + H_3)^3}{12}}{(1 - \nu_1^2)\rho_1(H_1 + H_2 + H_3)} \quad (78)$$

where the only unknowns are the wavenumbers k_I . The estimated wavenumbers, which are needed in Eqs. (66) and (77), are presented in Table 5.

Finally, following the iterative process shown in Section 3.4.2, the effective thickness, the natural frequencies and the loss factors corresponding to the first 8 modes were estimated with Eqs. (66) and (77), respectively. The effective thickness for each mode, which is complex, is shown in Table 6, whereas the natural frequencies and loss factors are presented in Table 5. It has been considered that loss factor and the modal damping ratio ζ are related by [47]:

$$\eta = 2 \cdot \zeta \quad (79)$$

1
2
3
4 It can be seen that the natural frequencies can be estimated with an error of less than 8%
5 for all the modes considered in the investigation. Moreover, the type of supports does
6 not significantly affect the experimental natural frequencies of the plate.
7
8
9

10 With respect to the experimental loss factors (Table 3), the discrepancies between the
11 results found with wooden supports and with steel supports were less than 12%. On the
12 other hand, larger discrepancies were found between the experimental and the predicted
13 loss factors (Table 5).
14
15
16

17 The estimation of damping in structural systems is the most complex problem in
18 structural dynamics. Unlike the mass and stiffness characteristics of a structural
19 systems, damping does not relate to a single physical phenomenon and there are as
20 many damping mechanisms as there are modes converting mechanical energy into heat
21 [48]. In laminated-glass elements, the material damping contribution comes mainly
22 from the interlayer and the contribution of glass to damping is usually neglected in the
23 analytical models [18-24]. However, this contribution also depends on the material used
24 for the interlayer. In case of PVB, the contribution of the glass to damping over 20°C
25 can be neglected, but its effect should be taken into account under this temperature.
26
27
28
29
30
31
32
33

34 The mechanical characterization of the interlayer is a key step in making good damping
35 predictions in laminated-glass elements. Although major efforts have been made in the
36 last years in order to improve the analytical modeling of viscoelastic materials, as well
37 as the testing and the fitting of the experimental results, the material properties are not
38 estimated with reasonable accuracy to allow a good estimation of the damping in
39 laminated-glass elements. In fact, the material properties proposed by several authors
40 [50] are clearly different and lead to widely discrepant results. On other occasions, the
41 material properties are good for static loadings but not for dynamic loadings. Another
42 damping contribution is the interfacial damping mechanism, i.e. the friction between
43 members, connections, and supports of a structural system. Aerodynamic damping is
44 also experienced by a structure vibrating in air [48]. Moreover, the proposed model for
45 plates has been extended from a model for beams. All these facts explain why the
46 uncertainty in the loss factors is so high. However, as mentioned in this paper, this is not
47 exclusive of laminated glass but also of other materials and structural systems.
48
49
50
51
52
53
54
55
56
57
58
59
60
61
62
63
64
65

1
2
3
4 Table 5 shows that the predicted damping augments with increasing frequency as is the
5 case in beams. However, this is not true of the tested plate where the modes 2, 3, 5, 7,
6 and 8 (bending + torsion) follow a different trend from that of modes 1, 4, and 6
7 (bending in one or two directions). Modes 2, 3, 5, 7, and 8 present errors less than 50%,
8 which is of the same order of error reported by the authors in previous tests performed
9 on laminated-glass beams [9]. For modes 1, 4, and 6, the error is significantly larger.

10
11
12
13
14
15 Regarding the mode shapes, the modal assurance criterion (MAC) [49] between the
16 experimental mode shapes and those corresponding to the monolithic elastic FEM
17 model, are shown in Table 7. It can be concluded that the experimental mode shapes of
18 the laminated-glass plate agree well with those of the FEM monolithic model—that is,
19 the mode shapes of laminated-glass plate are very similar to those of a monolithic plate
20 with the same dimensions and supports as those of the laminated-glass plate.
21
22
23
24
25

26
27 Table 8 presents the predictions with Eq. (38) and Eq. (77). Both equations provide
28 similar natural frequencies (differences less that 0.2%) and the maximum discrepancies
29 in the loss factors are around 5%.
30
31

32 33 *5.2 Laminated-glass beam*

34
35
36 The modal parameters of the laminated-glass beam were also predicted using Eq. (35).
37 The same material properties as those described for the plates were considered for the
38 beam.
39
40

41
42 As in the laminated-glass plate, the modal parameters of the laminated-glass beam were
43 estimated using the dynamic-effective-thickness concept. The initial natural frequencies
44 for the beam were estimated from the equation:
45
46
47
48
49

$$50 \quad \omega_0^2 = \frac{k_1^4 E \left(\frac{H_1^3 + H_3^3 + (H_1 + H_2 + H_3)^3}{24} \right)}{\bar{m}} \quad (80)$$

51
52
53
54
55
56 Where the wavenumbers k_1 are those of an Euler Bernoulli beam, which can be easily
57 found in the literature [27].
58
59
60
61
62
63
64
65

1
2
3
4 Then, the effective thickness, the natural frequencies, and the loss factors were
5 estimated following the iterative process indicated in section 3.4, but estimating
6 $H_{eff}(\omega)$ with the expression presented in Table 2. The predictions for the first three
7 modes in the temperature range $12 - 45\text{ }^{\circ}\text{C}$ is shown in Table 4. Very good agreement
8 exists for the natural frequencies at all the temperatures, the discrepancies being less
9 than 7%. It can be seen that the natural frequencies decrease as temperature increases
10 and this tendency is expected because the modulus of the PVB declines with rising
11 temperatures (Figure 2). Moreover, at temperatures below $20\text{ }^{\circ}\text{C}$, the wavenumber is
12 close to that corresponding to an Euler-Bernoulli beam, and Eq. (35) can be used to
13 accurately predict the natural frequencies on a laminated-glass beam at these
14 temperatures [9].
15

16
17 With respect to the loss factor, large discrepancies were encountered between the results
18 provided by the analytical model and the experimental results, the error being less than
19 50%. From Table 4, it is inferred that the maximum loss factors are reached in the
20 range $40 - 50\text{ }^{\circ}\text{C}$, whereas damping is very small at low temperatures.
21

22
23 Regarding the mode shapes, again a very good correlation exists between the mode
24 shapes of the laminated-glass beam and those corresponding to a monolithic beam, the
25 MAC being very close to one for all the modes and all temperatures (Figure 8). Thus,
26 we can conclude that the effect of temperature in the mode shapes of a laminated-glass
27 beam element can be neglected.
28
29

30 31 32 33 34 35 36 37 38 39 40 41 42 43 44 45 6 CONCLUSIONS 46

47
48 In the practical calculations of laminated-glass elements, as well as in preliminary
49 designs, it is very useful to consider simplified methods. In recent years, several
50 equations have been proposed to calculate displacements, internal forces, stresses, etc.,
51 in laminated-glass beams and plates under static loading using the effective-thickness
52 concept [1, 3, 4, 8]. With this method, engineers can avoid the use of complex finite-
53 element models with small 3D elements which are exceedingly time consuming. The
54 effective thickness can also be used to check the results found with numerical models. If
55
56
57
58
59
60
61
62
63
64
65

1
2
3
4 the core is viscoelastic, the static effective thickness is time and temperature dependent.
5
6 It has been demonstrated that this technique provides reasonably accurate results in
7
8 beams and rectangular plates under common loadings and boundary conditions [3, 4,
9
10 37].

11 Aenlle and Pelayo [9] derived an effective thickness for the dynamic behavior of
12
13 laminated-glass beams based on the model of Ross, Ungar, and Kerwin [18, 19]. The
14
15 natural frequencies and the loss factors for laminated-glass beams are estimated using
16
17 Eq. (35) whereas the mode shapes are considered equal to those of the monolithic beam
18
19 with the same boundary conditions. The dynamic effective thickness is frequency and
20
21 temperature dependent and an iterative process has to be followed to estimate the modal
22
23 parameters. However, convergence is achieved in less than four iterations.

24 The conclusions of the paper are:

- 25
26 1. A dynamic effective thickness is proposed for rectangular laminated-glass plates
27
28 based on the relationship between the static and the dynamic stiffness derived by
29
30 the authors [9] for laminated-glass beams. Only one dynamic effective thickness
31
32 (frequency and temperature dependent) is needed to estimate the natural
33
34 frequencies and the loss factors of rectangular laminated-glass plates. With
35
36 respect to the mode shapes, it is inferred from the experiments and the analytical
37
38 models that they can be considered (without significant loss of accuracy), equal
39
40 to those of the corresponding monolithic model (same dimensions and boundary
41
42 conditions)
- 43
44 2. In monolithic beams, the buckling length, and the wavelength of the mode
45
46 shapes depend on the bending stiffness EI , which is constant in statics and
47
48 dynamics. In laminated-glass beams, the static and dynamic effective stiffnesses
49
50 (Eqs. (10) and (39)) are given by different expressions but the only difference
51
52 (apart from time and frequency) are the parameters ψ_B and k_I . The same
53
54 conclusion applies to static and the dynamic effective thicknesses.

55
56 It has been demonstrated that the parameter ψ_B is related to the buckling length
57
58 of beam under constant compression (Eq. (52)), whereas k_I is related to the
59
60 wavelength λ of the mode shapes. This means that, in the same way as in
61
62 monolithic beams, the buckling length (buckling wavelength) is related to the
63
64
65

1
2
3
4 static effective stiffness and the wavelength of the mode shapes to the dynamic
5 effective stiffness, respectively, with the important difference that the stiffness is
6 time (or frequency) and temperature dependent in laminated-glass and constant
7 in the monolithic case.
8
9

- 10
11 3. In rectangular monolithic plates, the wavelength of the mode shapes and the
12 dimension of the buckling wavelength, are also related to the stiffness D .
13

14
15 It has been also demonstrated that, in the same way as the laminated-glass
16 beams, the parameter ψ_P for laminated-glass plates is related to the dimension of
17 the waves that a plate buckles into when it is subject to constant compressive
18 loading on all the borders.
19

20
21 The relationship that exists in laminated-glass beams between the static
22 parameter ψ_B and the wavenumber k_I , is extended to the two-dimensional case
23 of rectangular glass plates but considering the parameters ψ_P and the
24 wavenumbers k_I corresponding to plates.
25

- 26
27 4. The concept of effective Young modulus is proposed as an alternative to
28 effective thickness, which can also be derived from the effective stiffness. The
29 effective Young modulus is more appealing for use in numerical and analytical
30 models because the monolithic model has constant thickness whereas a time- (or
31 frequency-) and temperature-dependent Young modulus is defined.
32

- 33
34 5. In order to validate the methodology, the modal parameters of a laminated-glass
35 plate 1400 x 1000 x 16 mm, with annealed glass and PVB core, pin supported at
36 the four corners, were estimated using the dynamic effective thickness. The
37 wavenumbers needed in Eq. (62) were estimated from a monolithic finite-
38 element model assembled in ABAQUS. The natural frequencies and the loss
39 factors were estimated with Eq. (77) whereas the mode shapes were considered
40 equal to those of the monolithic model.
41

42
43 The analytical predictions were validated by operational modal analysis and the
44 experimental results show that good accuracy is attained in the natural
45 frequencies (error less than 7%) but high scatter is achieved in the loss factors.
46 However, it is not possible to discriminate whether this large error in the loss
47 factors is due to inaccuracies of the model or to a poor mechanical
48
49
50
51
52
53
54
55
56
57
58
59
60
61
62
63
64
65

1
2
3
4 characterization of the core material (PVB). Furthermore, it has inferred from
5 the experiments that the type of supports used in tests do not significantly affect
6 the damping.
7

8
9 With respect to the mode shapes, the modal assurance criteria (MAC) between
10 the predicted and the experimental mode shapes are very close to unity for all
11 the modes, indicating a very good correlation.
12
13

- 14
15 6. With the purpose of validating the model for different temperatures and
16 boundary conditions, the modal parameters of a free-free laminated-glass beam
17 in the temperature range from 12 to 45 °C and with the geometrical data $L =$
18 1 m , $H_1 = 3.75 \text{ mm}$, $H_2 = 0.38 \text{ mm}$, $H_3 = 7.90 \text{ mm}$, $b = 0.1 \text{ m}$, were
19 estimated using the effective-thickness concept. The results were validated by
20 operational modal tests conducted in a climate chamber at temperatures from 12
21 to 45 °C. Good accuracy was achieved in the natural frequencies (error less than
22 7%) whereas the maximum error in the loss factors was around 50%. With
23 respect to the mode shapes, again the MAC is very close to unity for all the
24 modes at all the temperatures, which means that the mode shapes are not
25 affected significantly by temperature.
26
27
28
29
30
31
32
33

34 35 36 37 38 ACKNOWLEDGMENTS

39
40 The economic support given by the Spanish Ministry of Education through the project
41 BIA2011-28380-C02-01 is gratefully appreciated.
42
43
44
45
46
47
48
49
50
51
52
53
54
55
56
57
58
59
60
61
62
63
64
65

1
2
3
4 REFERENCES
5
6

7 [1] Benninson, S., M.HX, Q. and Davies, P., High-performance laminated glass for
8 structurally efficient glazing. Innovative Light-weight Structures and Sustainable
9 Facades, Hong Kong, May, 2008.
10

11
12
13 [2] Norville, H.S., King, K.W., and Swoord, J.L., Behavior and strength of laminated
14 glass,” J Eng Mech. 1998;124(1):46-53.
15

16
17 [3] Galuppi, L., and Royer-Carfagni, G.F., Effective Thickness of Laminated Glass
18 Beams: New Expression via a Variational Approach, J Struct Eng, 2012;38:53-67.
19
20

21
22 [4] Galuppi, L., and Royer-Carfagni, G.F., The Effective Thickness of Laminated Glass
23 Plates, J Mech Mater Struct ures, 2012;7(4):375-400.
24
25

26
27 [5] Ivanov, I.V., Analysis, Modeling and Optimization of Laminated Glasses as Plane
28 Beam, Int J Solids Struct, 2006;43(22-23):6887-6907.
29
30

31 [6] Koutsawa, Y., and Daya, E.M., Static and Free Vibration Analysis of Laminated
32 Glass Beam on Viscoelastic Supports, Int J Solids Struct, 2007;44:8735-8750.
33
34

35
36 [7] Asik, M.Z., Tezcan, S., A Mathematical Model for the Behavior of Laminated Glass
37 Beams, Comput Struct. 2005;83:1742-1753.
38
39

40 [8] Calderone, I., Davies, P.S., and Benninson, S.J., Effective Laminate Thickness for
41 the Design of Laminated Glass. In: *Glass Processing Days*, Tampere, Finland, 2009.
42
43

44
45 [9] López-Aenlle, M., Pelayo, F., Frequency Response of Laminated Glass Elements:
46 Analytical Modelling and Effective Thickness, Appl Mech Rev, 2013;65(2), 020802 (13
47 pages).
48
49

50
51 [10] Foraboschi P., Analytical Solution of two layer beam taking into account nonlinear
52 interlayer slip. ASCE J. Eng. Mech., 2009, 135(10), 1129-1146.
53
54

55
56 [11] Benninson, S.J., Jagota, A., and Smith, C.A., Fracture of Glass/pvb Laminates in
57 Biaxial Flexure, J Am Ceram Soc, 1999;82(7):1761-1770.
58
59

- 1
2
3
4 [12] Lee, E.H., Stress Analysis in Viscoelastic Bodies, Q J Mech Appl Math,
5 1955;13:183-190.
6
7
8 [13] Read, W.T., Stress Analysis for Compressible Viscoelastic Materials. J Appl Phys,
9 1950;21:671-674.
10
11
12 [14] Ferry, J.D., Viscoelastic Properties of Polymers, Third ed., John Wiley & Sons,
13 Ltd., New York. 1980.
14
15
16 [15] Williams, M.L., Landel, R.F., and Ferry, J., The Temperature Dependence of
17 Relaxation Mechanisms in Amorphous Polymers and Other Glass-forming Liquids, J
18 Am Chem Soc, 1955;77:3701-3707.
19
20
21 [16] Tschoegl, N.W., The Phenomenological Theory of Linear Viscoelastic Behavior,
22 Springer-Verlag, Berlin. 1989.
23
24
25 [17] Foraboschi, P., Analytical model for laminated-glass plate, Compos Part B-Eng,
26 2012;43(5):2094-2106.
27
28
29 [18] Kerwin, E.M., Damping of Flexural Waves by a Constrained Viscoelastic Layer, J.
30 Acoust. Soc. Am, 1959;31(7):952-962.
31
32
33 [19] Ross, D., Ungar, E.E., and Kerwin, E.M., Damping of Plate Flexural Vibrations by
34 Means of Viscoelastic Laminate, Structural Damping, ASME, 1959; p. 49-88.
35
36
37 [20] DiTaranto, R.A., and McGraw, Jr, J.R., Vibratory Bending of Damped Laminated
38 Plates, J Eng Ind, 1969;91(4):1081-1090.
39
40
41 [21] DiTaranto, R.A., Theory of Vibratory Bending for Elastic and Viscoelastic Layered
42 Finite-Length Beams, J Appl Mech, 1965;32:881-886.
43
44
45 [22] Mead, D.J., and Markus, S., The Forced Vibration of a Three-Layer, Damped
46 Sandwich Beam with Arbitrary Boundary Conditions, J Sound Vib, 1969;10(2):163-
47 175.
48
49
50
51
52
53
54
55
56
57
58
59
60
61
62
63
64
65

- 1
2
3
4 [23] Mead D.J., and Markus, S., Loss Factors and Resonant Frequencies of Encastred
5 Damped Sandwich Beam, *J Sound Vib*, 1970;12(1):99-112.
6
7
8
9 [24] Rao, D.K., Frequency and Loss Factors of Sandwich Beams under Various
10 Boundary Conditions, *J Mech Eng Sci*, 1978;20(5):271-282.
11
12
13 [25] Foraboschi, P., Behavior and Failure Strength of Laminated Glass Beams. *J Eng*
14 *Mech. (ASCE)*, 2007;133:1290-1301.
15
16
17 [26] Foraboschi, P., Three-layered sandwich plate: Exact mathematical model. *Compos*
18 *Part B-Eng*, 2013;45:1601-1612
19
20
21
22 [27] Foraboschi, P., Three-layered plate: Elasticity solution. *Compos Part B-Eng*, in
23 *press*, 2014.
24
25
26
27 [28] Foraboschi, P., Layered plate with discontinuous connection: Exact mathematical
28 *model. Compos Part B-Eng*, 2013;47:365-378.
29
30
31
32 [29] Foraboschi, P., Hybrid Laminated-Glass plate: Design and assessment. *Compos*
33 *Struct*, 2013; 106:250-263.
34
35
36 [30] D'Ambrisi, A., Feo, L., Focacci, F., Bond-slip relations for PBO-FRCM materials
37 *externally bonded to concrete. Compos Part B-Eng*, 2012; 43(8):2938-2949.
38
39
40
41 [31] D'Ambrisi, A., Feo, L., Focacci, F., Experimental analysis on bond between PBO-
42 *FRCM strengthening materials and concrete. Compos Part B-Eng*, 2013; 44(1): 524-
43 *532.*
44
45
46
47 [32] D'Ambrisi, A., Feo, L., Focacci, F., Experimental and analytical investigation on
48 *bond between Carbon-FRCM materials and masonry. Compos Part B-Eng*, 2013; 46:15-
49 *20.*
50
51
52
53 [33] Labuz, J.F., Biolzi, L., Characteristic strength of quasi-brittle materials. *Int J Solids*
54 *Struct*. 1998; 35(31-32):4191-4203.
55
56
57
58
59
60
61
62
63
64
65

- 1
2
3
4 [34] Biolzi, L., Cattaneo, S., Rosati, G., Progressive damage and fracture of laminated
5 glass beams, *Constr Build Mater*, 2010; 24(4):577-584.
6
7
8
9
10
11 [35] Foraboschi, P., Laminated glass column, *Int J Struct Eng*, 2009;87:20-26.
12
13
14 [36] Wölfel, E., Nachgiebiger Verbund Eine Näherungslösung und deren
15 Anwendungsmöglichkeiten, In: *Stahlbau*, 1987;6:173-180.
16
17
18 [37] Galuppi, L., Manara, G. and Royer-Carfagni, G., Practical expressions for the
19 design of laminated glass. *Compos Part B-Eng*, 2013;45:1677-1688.
20
21
22
23 [38] Wang, C.M., Vibration Frequencies of Simply Supported Polygonal Sandwich
24 Plates via Kirchhoff Solutions. *J Sound Vib*, 1996;190(2):255-260.
25
26
27
28 [39] Blevins, R.D., *Formulas for natural Frequency and Mode Shapes*, Krieger
29 Publishing Company, Malabar, Florida, 2001.
30
31
32 [40] Nashif, A.D., Jones, D.I.G., and Henderson, J.P., *Vibration Damping*. John Willey
33 and Sons, New York. 1985.
34
35
36
37 [41] Blasón, S., López-Aenlle, M., Pelayo, F., Influence of Temperature on the Modal
38 Parameters of Laminated Glass Beams, In *Proc. Of the International Conference on*
39 *Vibration Problems (ICOVP13)*. Lisbon, 2013, paper-504, p. 270.
40
41
42
43 [42] López-Aenlle, M., Pelayo, F., Villa, L.M., Barredo, J., Hermanns, L. and Fraile, A.,
44 Operational Modal Analysis on Laminated Glass Beams. In *proc. Of the 4th*
45 *International Operational Modal Analysis Conference (IOMAC11)*. Istanbul, 2011.
46
47
48
49 [43] Pelayo, F., López-Aenlle, M., Hermanns, L. and Fraile, A., Modal Scaling of a
50 Laminated Glass Plate. In *Proc. Of the 5th International Operational Modal Analysis*
51 *Conference (IOMAC)*, Guimaraes, 2013, paper 175.
52
53
54
55
56
57
58
59
60
61
62
63
64
65

1
2
3
4 [44] Brincker, R., Zhang, L-M., and Andersen. P., Modal Identification from Ambient
5 Response Using Frequency Domain Decomposition, in: Proceedings of the 18th
6 International Modal Analysis Conference (IMAC), San Antonio, 2000, p. 625-630.
7
8
9

10 [45] Pelayo, F., López-Aenlle, M., Brincker, R. and Fernández-Canteli, A., Artificial
11 Excitation in Operational Modal Analysis, In Proc. Of the 3th International Operational
12 Modal Analysis Conference (IOMAC). Portonovo, Ancona. 2009, Paper 223.
13
14
15

16 [46] Van Overschee, P., and De Moor, B., Subspace Identification for Linear Systems:
17 Theory, Implementation & Applications, Dordrecht, Netherlands, Kluwer Academic
18 Publishers. 1996.
19
20
21

22 [47] Wanbo, L., Experimental and Analytical Estimation of Damping in Beams and
23 Plates with Damping Treatments, Ph.D. Thesis, University of Kansas, 2008.
24
25
26

27 [48] Kareem, A. and Gurley, K., Damping in structures: its evaluation and treatment of
28 uncertainty, J Wind Eng Ind Aerod, 1996;56:131-157.
29
30
31

32 [49] Ewins, D.J., Modal testing: theory, practice and application. Second Ed. Research
33 Studies Press, LTD. John Willey and Sons, LTD. England, 2000.
34
35
36

37 [50] Feldmann, M., Kasper, R. et al. Guidance for European Structural Design of Glass
38 Components. JCR Scientific and Policy Report, doi: 10.2788/5523, 2014.
39
40
41
42
43
44
45
46
47
48
49
50
51
52
53
54
55
56
57
58
59
60
61
62
63
64
65

1
2
3
4
5
6
7
8
9
10
11
12
13
14
15
16
17
18
19
20
21
22
23
24
25
26
27
28
29
30
31
32
33
34
35
36
37
38
39
40
41
42
43
44
45
46
47
48
49
50
51
52
53
54
55
56
57
58
59
60
61
62
63
64
65

FIGURE CAPTIONS:

Figure 1: Laminated glass.

Figure 2: Tensile and shear moduli of PVB at 20°C.

Figure 3. Estimation of natural frequencies and loss factors using methodology I.

Figure 4. Estimation of natural frequencies and loss factors using methodology II.

Figure 5. Test setup of the plate. a) Picture of the plate without sensors. b) Location of the accelerometers (arrows show accelerometers direction).

Figure 6. a) Detail of the wooden support. b) Detail of the steel support.

Figure 7. Test setup of the beam (arrows show accelerometers direction).

Figure 8. MAC between the experimental and analytical mode shapes at different temperatures.

1
2
3
4
5
6
7
8
9
10
11
12
13
14
15
16
17
18
19
20
21
22
23
24
25
26
27
28
29
30
31
32
33
34
35
36
37
38
39
40
41
42
43
44
45
46
47
48
49
50
51
52
53
54
55
56
57
58
59
60
61
62
63
64
65

1
2
3
4
5
6
7
8
9
10
11
12
13
14
15
16
17
18
19
20
21
22
23
24
25
26
27
28
29
30
31
32
33
34
35
36
37
38
39
40
41
42
43
44
45
46
47
48
49
50
51
52
53
54
55
56
57
58
59
60
61
62
63
64
65

TABLE CAPTIONS

- Table 1. Static effective thickness and effective Young modulus for laminated-glass beams and plates.
- Table 2. Dynamic effective thickness and effective Young modulus for laminated-glass beams.
- Table 3. Experimental modal parameters for the plate.
- Table 4. Experimental and predicted natural frequencies and loss factors for the beam
- Table 5. Comparison of experimental and predicted modal parameters for the plate.
- Table 6. Effective thicknesses for the plate at 20.5 °C.
- Table 7. Mode shapes and MAC between experimental and FE model for the plate.
- Table 8. Comparison of predicted modal parameters for the plate with Eqs. (38) and (77).

Table1

Model		Equation
Benninson et al. (beams)	$E_1 = E_3$	$H_{eff}(t) = \sqrt[3]{(H_1^3 + H_3^3)(1 + \Gamma_S(t)Y_1)}$
		$E_{eff}(t) = \frac{E_1(H_1^3 + H_3^3)(1 + \Gamma_S(t)Y_1)}{H^3}$
	$E_1 \neq E_3$	$H_{1eff}(t) = \sqrt[3]{\left(H_1^3 + H_3^3 \frac{E_3}{E_1}\right) (1 + \Gamma_S(t)Y)}$
		$H_{3eff}(t) = \sqrt[3]{\left(\frac{E_1}{E_3} H_1^3 + H_3^3\right) (1 + \Gamma_S(t)Y)}$
		$E_{eff}(t) = \frac{(E_1 H_1^3 + E_3 H_3^3)(1 + \Gamma_S(t)Y)}{H^3}$
	Galuppi et al. (beams)	$E_1 = E_3$
$E_{eff}(t) = \frac{E_1(H_1^3 + H_3^3)(1 + Y_1)}{H^3 1 + Y_1(1 - \eta_{S1}(t))}$		
$E_1 \neq E_3$		$H_{1eff}(t) = \sqrt[3]{\frac{12EI_T(1 + Y)}{E_1(1 + Y(1 - \eta_S(t)))}}$
		$H_{3eff}(t) = \sqrt[3]{\frac{12EI_T(1 + Y)}{E_3(1 + Y(1 - \eta_S(t)))}}$
		$E_{eff}(t) = \frac{12EI_T(1 + Y)}{H^3(1 + Y(1 - \eta_S(t)))}$
Galuppi et al. (plates)		$E_1 \neq E_3$

		$E_{eff}(t) = \frac{12(1 - v_{eff}^2)(D_1 + D_3)(1 + Y_p)}{H^3(1 + Y_p(1 - \eta_{SP}(t)))}$

Table2

Model		Equation
General	$E_1 \neq E_3$	$H_{1eff}(\omega) = \sqrt[3]{\left(H_1^3 + H_3^3 \frac{E_3}{E_1}\right) \left(1 + \frac{Y}{1 + \frac{E_1 H_1}{g_R^*(\omega)(E_1 H_1 + E_3 H_3)}}\right)}$
		$H_{3eff}(\omega) = \sqrt[3]{\left(\frac{E_1}{E_3} H_1^3 + H_3^3\right) \left(1 + \frac{Y}{1 + \frac{E_1 H_1}{g_R^*(\omega)(E_1 H_1 + E_3 H_3)}}\right)}$
		$E_{eff}(\omega) = \frac{(E_1 H_1^3 + E_3 H_3^3) \left(1 + \frac{Y}{1 + \frac{E_1 H_1}{g_R^*(\omega)(E_1 H_1 + E_3 H_3)}}\right)}{H^3}$
Galuppi et al.	$E_1 \neq E_3$	$H_{1eff}(\omega) = \sqrt[3]{\frac{\left(H_1^3 + H_3^3 \frac{E_3}{E_1}\right) (1 + Y)}{(1 + Y(1 - (\omega)))}}$
		$H_{3eff}(\omega) = \sqrt[3]{\frac{\left(\frac{E_1}{E_3} H_1^3 + H_3^3\right) (1 + Y)}{(1 + Y(1 - (\omega)))}}$
		$E_{eff}(\omega) = \frac{(E_1 H_1^3 + E_3 H_3^3) (1 + Y)}{H^3 (1 + Y(1 - (\omega)))}$

Table3

Mode	Natural Frequency			Loss Factor (η)		
	Experimental (Wooden supports)	Experimental (Steel supports)	Error	Experimental (Wooden supports)	Experimental (Steel supports)	Error
	[Hz]	[Hz]	[%]	[%]	[%]	[%]
1	18.59	18.71	-0.65	1.95	2.24	-12.54
2	42.34	42.61	-0.64	3.54	3.65	-3.11
3	48.34	48.91	-1.17	3.95	4.23	-7.08
4	65.4	66.07	-1.01	1.53	1.57	-2.32
5	101.3	102.91	-1.56	2.99	2.70	9.74
6	121	120.90	0.08	1.34	1.27	5.02
7	130	131.62	-1.23	2.83	3.10	-9.37
8	162.9	167.11	-2.52	3.88	3.93	-1.44

Temperature	Natural Frequencies			Loss Factor (η)		
	OMA	RKU	Error	OMA	RKU	Error
[°C]	[Hz]	[Hz]	[%]	[%]	[%]	[%]
Mode 1						
12	66.65	66.16	0.74	0.28	0.15	46.43
20	66.47	66.02	0.68	0.56	0.43	23.21
25	66.29	65.78	0.77	0.95	0.9	5.26
30	65.97	65.38	0.89	2.11	1.87	11.37
35	65.37	64.86	0.78	4.56	4.15	8.99
40	63.70	63.14	0.88	8.98	8.55	4.79
45	60.25	60.39	-0.23	18.91	13.44	28.93
Mode 2						
12	182.91	181.73	0.65	0.44	0.32	28.19
20	182.03	180.79	0.68	0.97	0.73	25.42
25	181.12	179.70	0.78	1.80	1.75	3.13
30	179.33	177.90	0.80	3.75	3.16	15.87
35	175.94	174.80	0.65	9.40	5.53	41.20
40	168.16	169.66	-0.89	22.98	12.14	47.17
45	153.72	157.9	-2.72	20.34	18.35	9.78
Mode 3						
12	357.10	354.38	0.76	0.50	0.51	-2.00
20	354.55	351.36	0.90	1.20	1.18	1.67
25	351.37	348.72	0.75	2.63	2.42	7.98
30	346.42	342.92	1.01	5.30	4.20	20.75
35	335.54	333.99	0.46	11.87	7.61	35.89
40	311.83	323.03	-3.59	19.54	13.13	32.80
45	276.82	295.70	-6.82	25.06	21.95	12.41

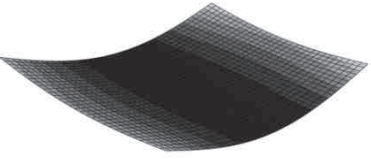
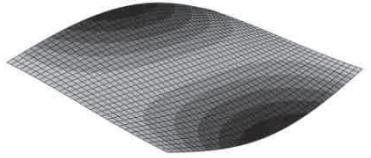
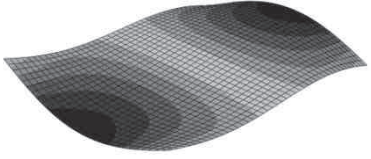
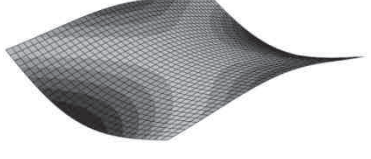
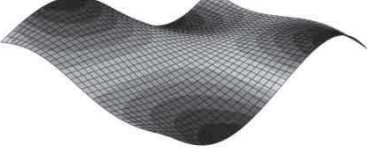
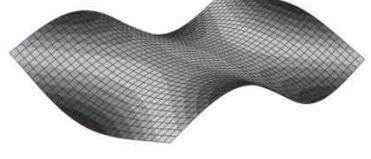
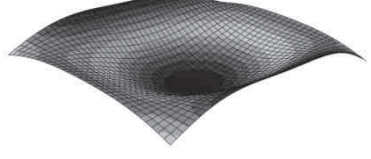
Table5

Mode	Wave-number	Natural Frequency			Loss Factor (η)		
		Eq. (77)	Experimental (Wooden support)	Error	Eq. (77)	Experimental (Wooden support)	Error
		[Hz]	[Hz]	[%]	[%]	[%]	[%]
1	2.103	18.32	18.59	-1.44	1.56	1.95	20.21
2	3.169	41.24	42.34	-2.65	2.52	3.54	28.76
3	3.455	48.91	48.34	1.17	2.74	3.95	30.79
4	3.888	61.71	65.4	-5.97	3.03	1.53	-97.09
5	5.010	101.33	101.3	0.04	3.79	2.99	-26.36
6	5.287	112.49	121	-7.57	3.99	1.34	-197.36
7	5.683	129.40	130	-0.46	4.31	2.83	-51.85
8	6.447	165.03	162.9	1.29	4.98	3.88	-28.33

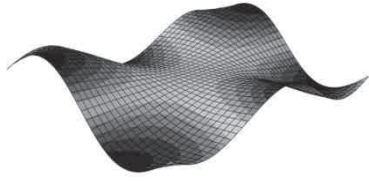
Table6

Mode	Effective Thickness [mm]	
	Real part	Imaginary part
1	16.2300	0.0843
2	16.1417	0.1357
3	16.1173	0.1471
4	16.0777	0.1626
5	15.9580	0.2014
6	15.9255	0.2119
7	15.8777	0.2280
8	15.7836	0.2619

Table 6: Mode shapes and MAC between experimental and FEM model for the plate.

Mode	Mode shape (FEM model)	MAC
1		0.9986
2		0.9887
3		0.9860
4		0.9981
5		0.9918
6		0.9993
7		0.9947

8

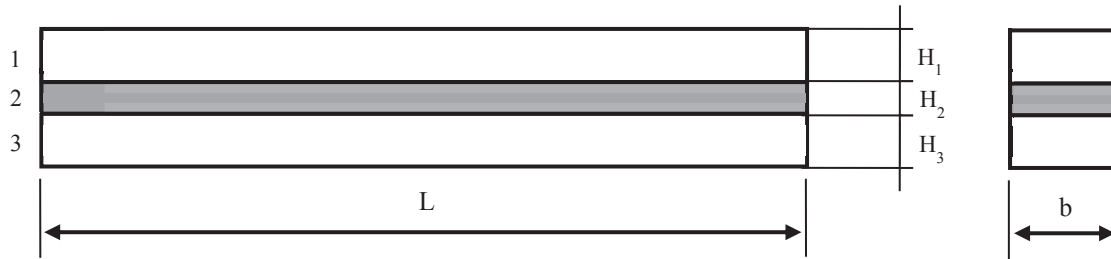


0.9913

Table8

Mode	Wave-number	Natural Frequency			Damping Ratio (η)		
		(Eq. 38)	(Eq. 77)	Error	(Eq. 38)	(Eq. 77)	Error
		[Hz]	[Hz]	[%]	[%]	[%]	[%]
1	2.103	18.33	18.32	-0.05	1.48	1.56	4.69
2	3.169	41.28	41.24	-0.09	2.40	2.52	4.59
3	3.455	48.96	48.91	-0.10	2.61	2.73	4.57
4	3.888	61.79	61.71	-0.12	2.89	3.03	4.53
5	5.010	101.51	101.33	-0.17	3.62	3.78	4.39
6	5.287	112.70	112.49	-0.19	3.82	3.99	4.35
7	5.683	129.67	129.40	-0.21	4.12	4.30	4.28
8	6.447	165.44	165.03	-0.25	4.77	4.98	4.15

Figure1



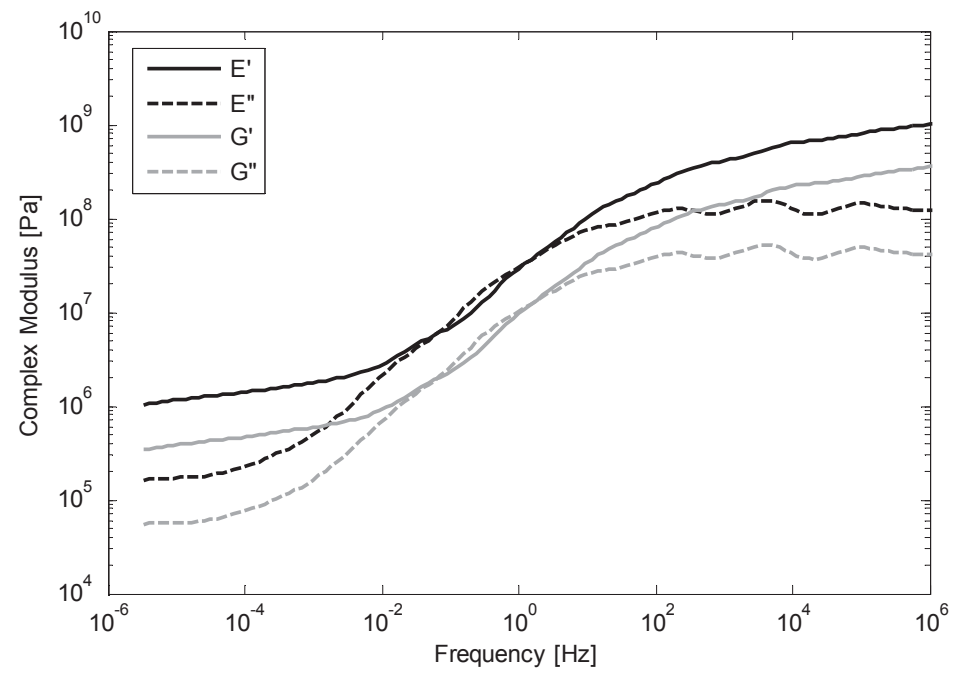


Figure3

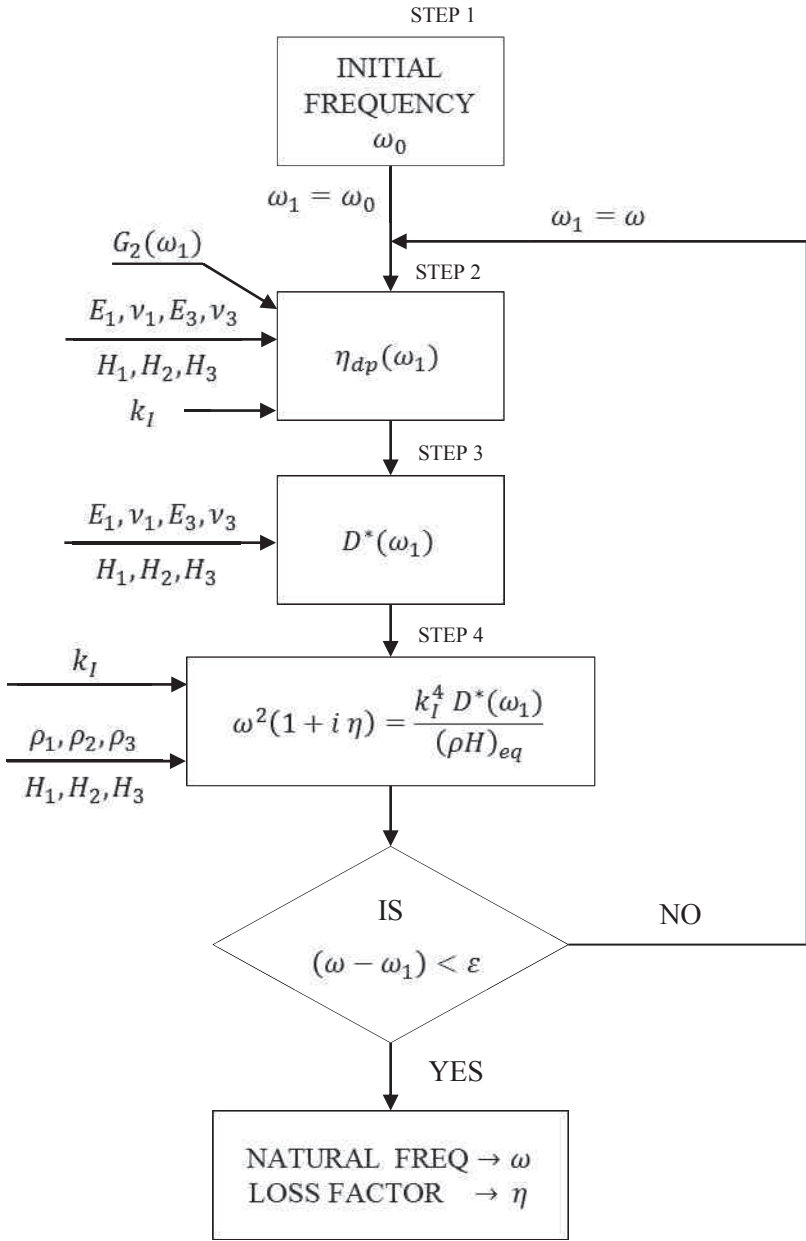


Figure4

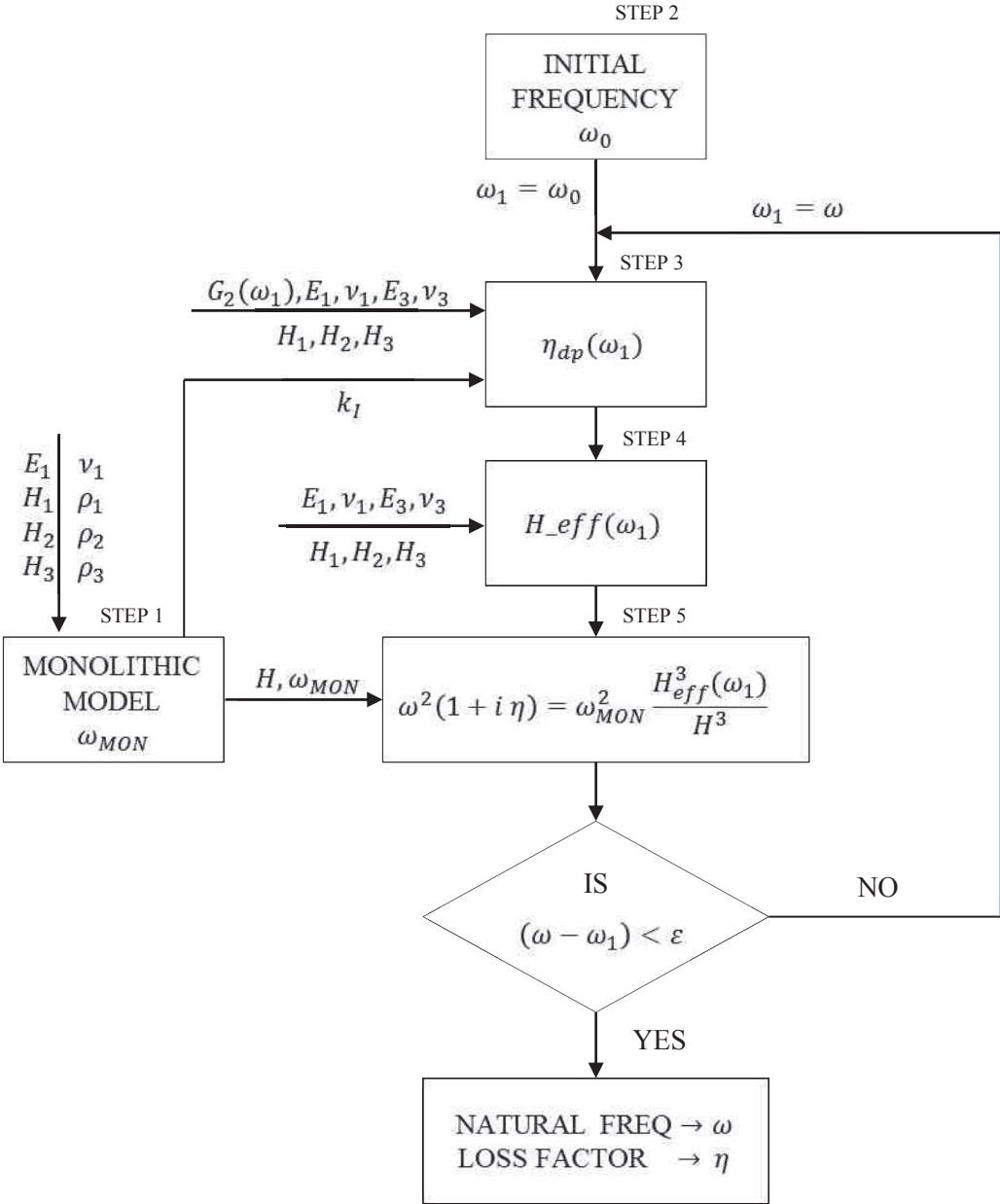


Figure5a
[Click here to download high resolution image](#)

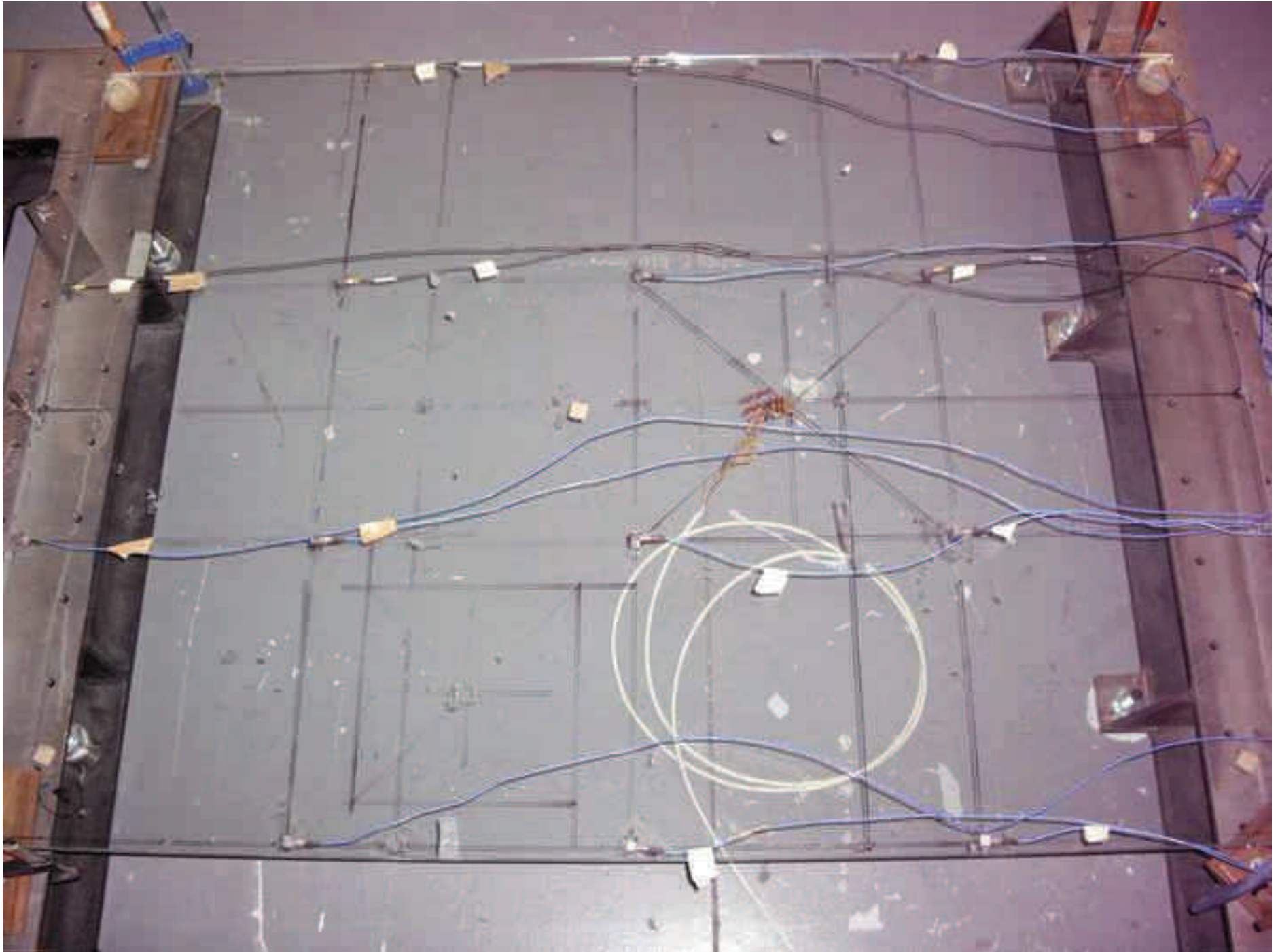


Figure5b

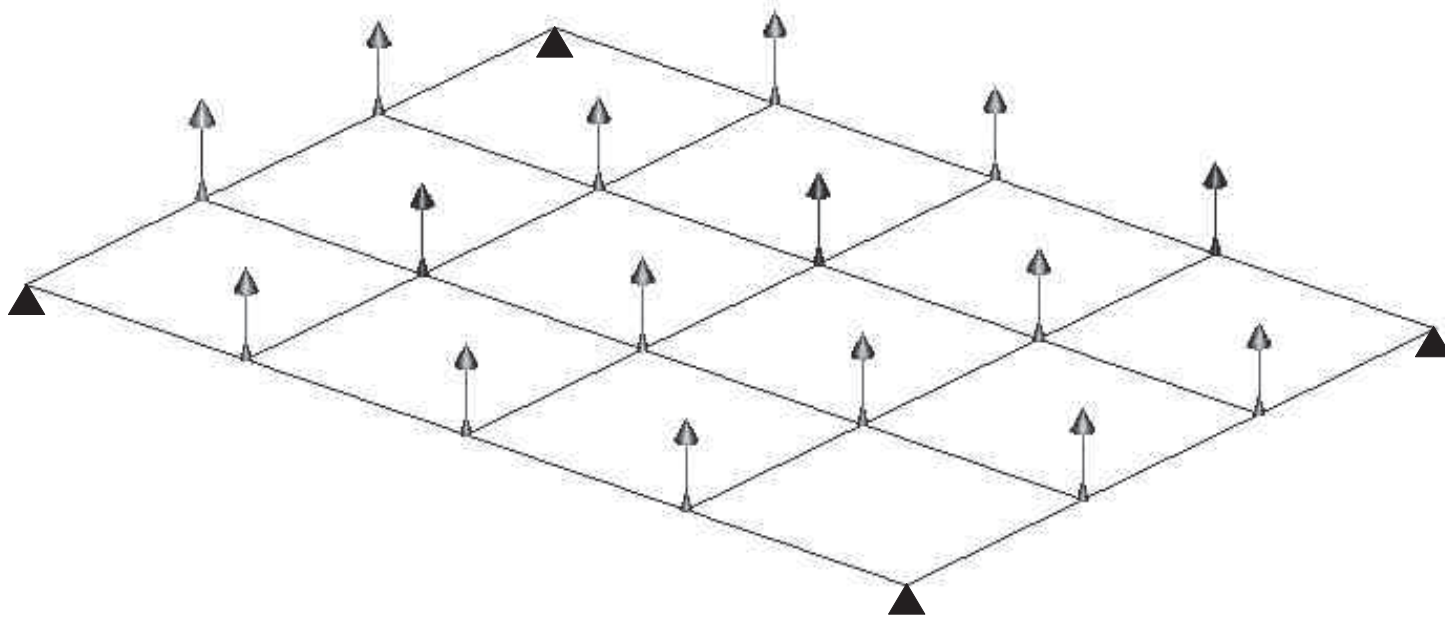


Figure6a
[Click here to download high resolution image](#)

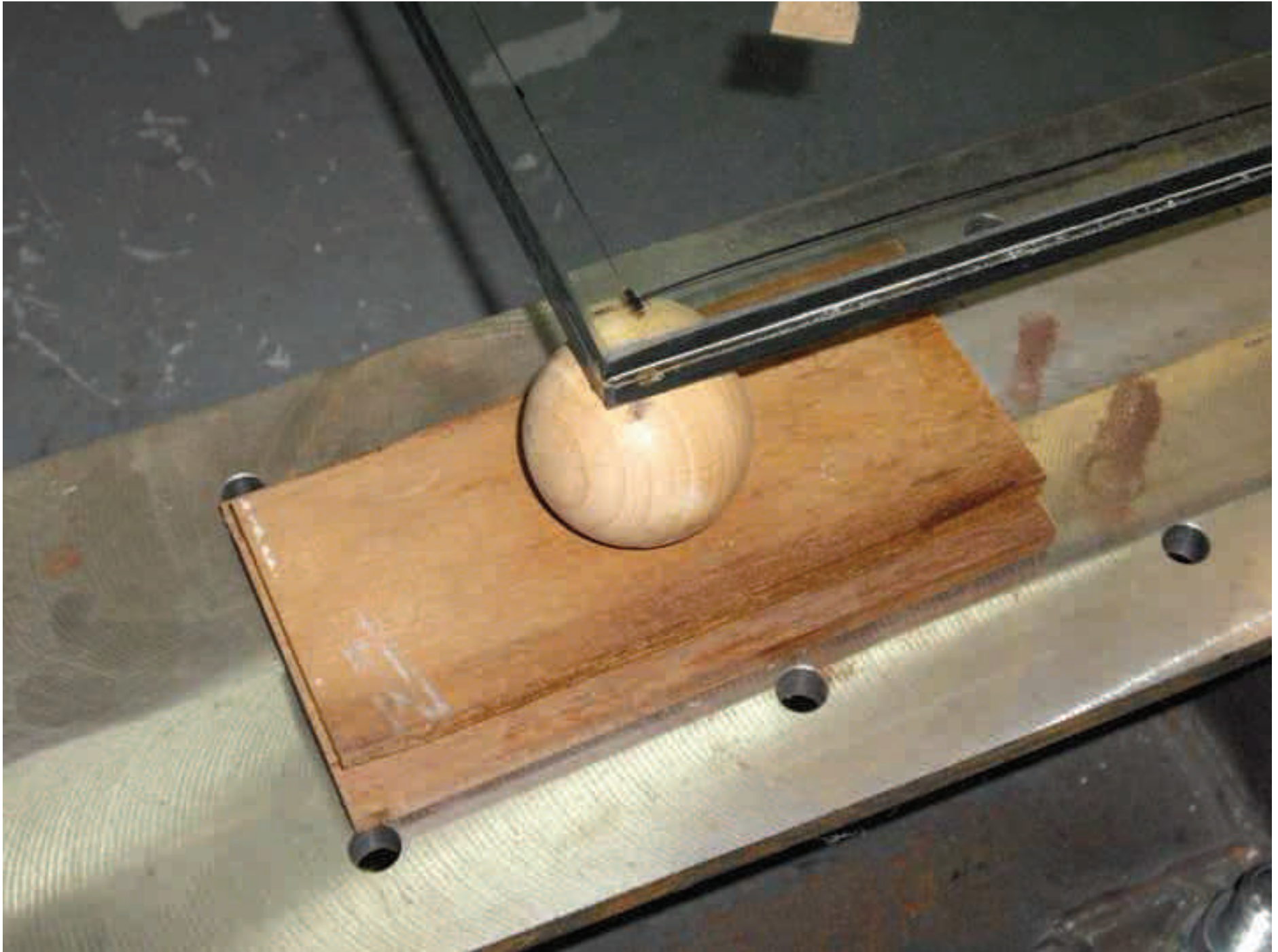


Figure6b
[Click here to download high resolution image](#)

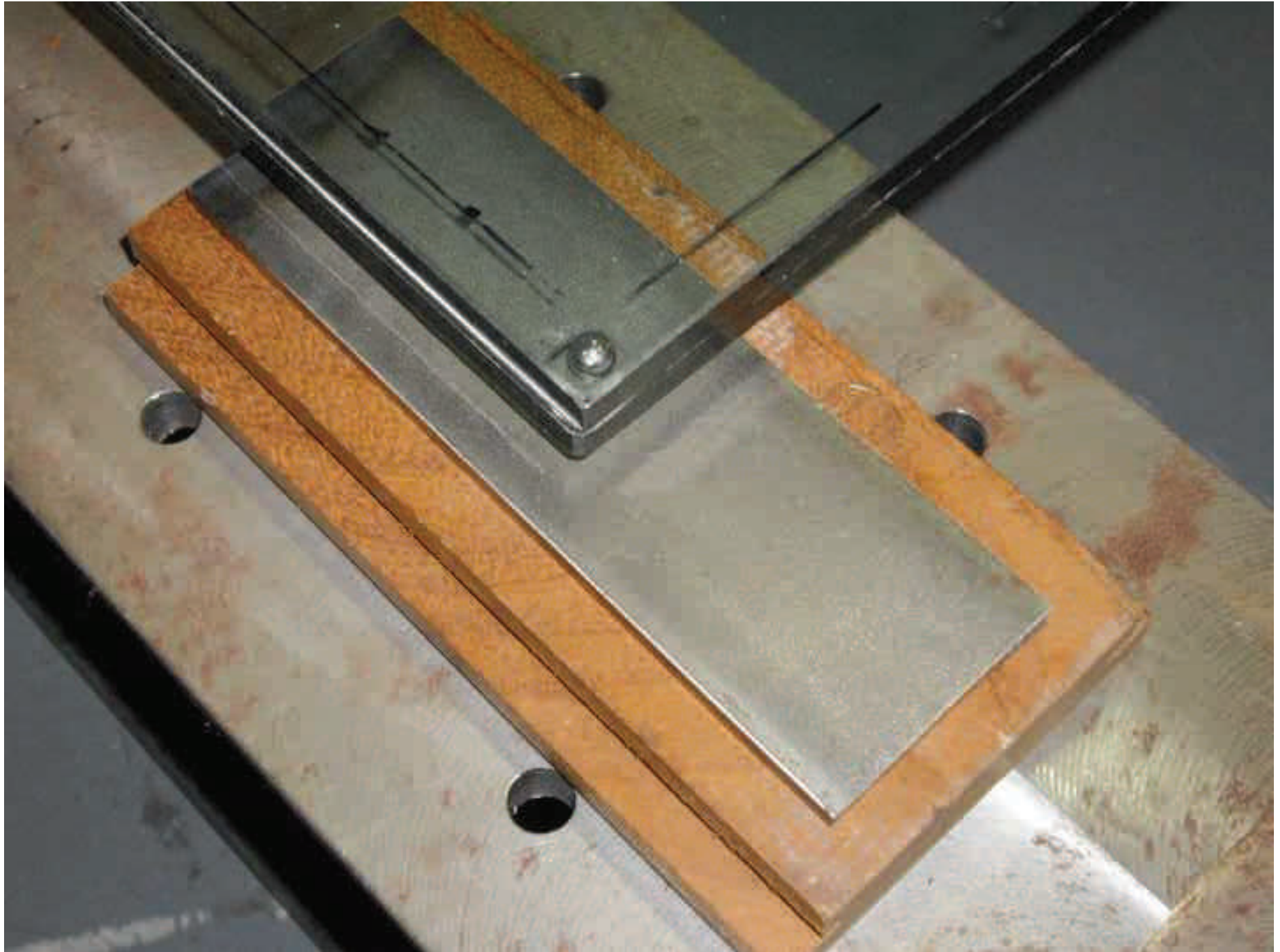


Figure 7

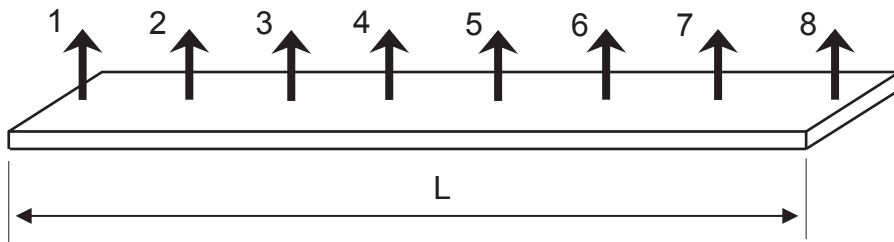


Figure8

